

석사 학위논문
Master's Thesis

비선형 동역학 문제에서의 뉴마크 시간적분
파라미터의 고찰

Insight into Newmark time integration parameters in non-linear dynamic problems



고 영 빈 (高瑛彬 Ko, Yeong-Bin)

기계항공시스템학부 해양시스템공학전공
School of Mechanical, Aerospace and Systems Engineering,
Division of Ocean Systems Engineering

KAIST

2013

Master's Thesis

Insight into Newmark time integration parameters in
non-linear dynamic problems



Ko, Yeong-Bin

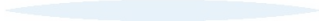
School of Mechanical, Aerospace and Systems Engineering

Department of Ocean Systems Engineering

KAIST

Insight into Newmark time integration parameters in
non-linear dynamic problems

KAIST

The logo for KAIST (Korea Advanced Institute of Science and Technology) is centered on the page. It consists of the letters 'KAIST' in a bold, blue, sans-serif font. Below the text is a light blue, horizontal, oval-shaped shadow or underline.

Insight into Newmark time integration parameters in non-linear dynamic problems

Advisor : Professor Lee, Phill-Seung

by

Ko, Yeong-Bin

School of Mechanical, Aerospace and Systems Engineering

Department of Ocean Systems Engineering

KAIST

A thesis submitted to the faculty of KAIST in partial fulfillment of the requirements for the degree of Master of Science in Engineering in the School of Mechanical, Aerospace and Systems Engineering, Department of Ocean Systems Engineering. The study was conducted in accordance with Code of Research Ethics¹

12, 20, 2012

Approved by

Professor Lee, Phill-Seung

[Advisor]

¹Declaration of Ethical Conduct in Research: I, as a graduate student of KAIST, hereby declare that I have not committed any acts that may damage the credibility of my research. These include, but are not limited to: falsification, thesis written by someone else, distortion of research findings or plagiarism. I affirm that my thesis contains honest conclusions based on my own careful research under the guidance of my thesis advisor.

비선형 동역학 문제에서의 뉴마크 시간적분 파라미터의 고찰

고 영 빈

위 논문은 한국과학기술원 석사학위논문으로
학위논문심사위원회에서 심사 통과하였음.

The logo for KAIST (Korea Advanced Institute of Science and Technology) is displayed in a light blue color. It consists of the letters 'KAIST' in a bold, sans-serif font, with a horizontal line underneath the letters.

2012 년 12 월 20 일

심사위원장 이 필 승 (인)

심사위원 박 광 춘 (인)

심사위원 오 일 권 (인)

MOSE

20113027

고 영 빈. Ko, Yeong-Bin. Insight into Newmark time integration parameters in non-linear dynamic problems. 비선형 동역학 문제에서의 뉴마크 시간적분 파라미터의 고찰. School of Mechanical, Aerospace and Systems Engineering, Department of Ocean Systems Engineering. 2013. 55p. Advisor Prof. Lee, Phill-Seung. Text in English.

ABSTRACT

In this study, we analyze nonlinear dynamic problems with numerical instability using Newmark (beta-2) time integration methods. By performing parameter study of Newmark method, we show that one parameter lead to numerical damping and the other parameter lead to period elongation only. Period elongation, unlike numerical damping, has been undiscovered as a role of stabilization in nonlinear dynamic problems. We validate our argument by numerical experiments including Newmark methods and Bathe's composite time integration method. We show that cases exist where numerical damping and period elongation have strength at accuracy over each other. This study gives us a motive for a better time integration method in the future, with wider range of characteristic including both period elongation and numerical damping.

Keywords: Newmark, time integration, Non-linear dynamics, Non-linear instability, Numerical damping, Period elongation

The logo for KAIST (Korea Advanced Institute of Science and Technology) is centered on the page. It consists of the letters "KAIST" in a bold, blue, sans-serif font. Below the text is a light blue horizontal oval shape that tapers at both ends, serving as a decorative underline.

Table of Contents

Abstract	i
Table of Contents	ii
List of Tables	iv
List of Figures	v
Chapter 1. Introduction	1
1.1 Finite Element Method in Nonlinear Dynamics	1
1.2 Nonlinear Instability	1
1.3 Implicit Time Integration Methods	2
Chapter 2. General Theory	4
2.1 Non-linear Formulation for structure	4
2.1.1 Basic Equation	4
2.1.2 Linearization of Basic Equation	7
2.1.3 Linearized Equation Including Dynamic Effect	9
2.2 Discretized Equation and Solution Procedure	9
Chapter 3. Time Integration Methods	11
3.1 Newmark Time Integration Method	11
3.2 Bathe composite Time Integration Method	14
3.3 Solution Process	15
3.4 Other Methods	16
Chapter 4. Numerical Results	17
4.1 Rotating Pendulum	17
4.1 Compound Pendulum	24
4.3 Cantilever Beam	33
4.4 Cylindrical Shell	40
Chapter 5. Conclusion	46
Appendix	47
Chapter A. Formulation of Shell Elements	48
References	54

Summary	56
Acknowledgement	57



List of Tables

3.1 Computation for equilibrium equation	15
4.1 Choice of parameter of numerical rotating pendulum for the evaluation of performance	18
4.2 Choice of parameter of numerical compound pendulum for the evaluation of performance	24
4.3 Choice of parameter of numerical cantilever beam for the evaluation of performance	33
4.4 Choice of parameter of numerical cylindrical shell for the evaluation of performance	41

The logo for KAIST (Korea Advanced Institute of Science and Technology) is centered on the page. It consists of the letters "KAIST" in a bold, blue, sans-serif font. Below the text is a light blue, horizontal oval shape that tapers at both ends, resembling a stylized shadow or a base.

List of Figures

2.1 Initial and current geometry of body of a structure	4
3.1 Spectral radius of Newmark method	13
3.2 Period elongation of Newmark method	13
4.1 Schema and description of the numerical rotating pendulum model	17
4.2 Velocity of the numerical rotating pendulum model using the trapezoidal rule, $EA = 10^{10} N$, $\Delta t = 0.01s$	19
4.3 Acceleration of the numerical rotating pendulum model using the trapezoidal rule, $EA = 10^{10} N$, $\Delta t = 0.01s$	19
4.4 Velocity of the numerical rotating pendulum model using two-substep Newmark(0.6,0.5) method, $EA = 10^{10} N$, $\Delta t = 0.5s$	20
4.5 Velocity of the numerical rotating pendulum model using Bathe composite method, $EA = 10^{10} N$, $\Delta t = 0.5s$	20
4.6 Acceleration of the numerical rotating pendulum model using two-substep Newmark(0.6,0.5) method, $EA = 10^{10} N$, $\Delta t = 0.5s$	21
4.7 Acceleration of the numerical rotating pendulum model using Bathe composite method, $EA = 10^{10} N$, $\Delta t = 0.5s$	21
4.8 Velocity of the numerical rotating pendulum model using two-substep Newmark(0.6,0.5) method, $EA = 10^3 N$, $\Delta t = 0.5s$	22
4.9 Velocity of the numerical rotating pendulum model using Bathe composite method, $EA = 10^3 N$, $\Delta t = 0.5s$	22
4.10 Acceleration of the numerical rotating pendulum model using two-substep Newmark(0.6,0.5) method, $EA = 10^3 N$, $\Delta t = 0.5s$	23
4.11 Acceleration of the numerical rotating pendulum model using Bathe composite method, $EA = 10^3 N$, $\Delta t = 0.5s$	23
4.12 Schema and description of the numerical compound pendulum model	24
4.13 Velocity of the numerical compound pendulum model using the trapezoidal rule, $E = 2 \times 10^{11} N/m^2$, $\Delta t = 0.005s$	25
4.14 Acceleration of the numerical compound pendulum model using the trapezoidal	

rule, $E = 2 \times 10^{11} \text{ N/m}^2$, $\Delta t = 0.005 \text{ s}$	26
4.15 Kinetic energy of the numerical compound pendulum model using the the trapezoidal rule, $E = 2 \times 10^{11} \text{ N/m}^2$, $\Delta t = 0.005 \text{ s}$. Straight reference line indicates initial potential energy.	26
4.16 Velocity of the numerical compound pendulum model using two-substep Newmark(0.6,0.5) method, $E = 6 \times 10^{11} \text{ N/m}^2$, $\Delta t = 0.05 \text{ s}$	27
4.17 Velocity of the numerical compound pendulum model using Bathe composite method, $E = 6 \times 10^{11} \text{ N/m}^2$, $\Delta t = 0.05 \text{ s}$	27
4.18 Acceleration of the numerical compound pendulum model using two-substep Newmark(0.6,0.5) method, $E = 6 \times 10^{11} \text{ N/m}^2$, $\Delta t = 0.05 \text{ s}$	28
4.19 Acceleration of the numerical compound pendulum model using Bathe composite method, $E = 6 \times 10^{11} \text{ N/m}^2$, $\Delta t = 0.05 \text{ s}$	28
4.20 Velocity of the numerical compound pendulum model using two-substep Newmark(0.6,0.5) method, $E = 1 \times 10^7 \text{ N/m}^2$, $\Delta t = 0.05 \text{ s}$	29
4.21 Velocity of the numerical compound pendulum model using Bathe composite method, $E = 1 \times 10^7 \text{ N/m}^2$, $\Delta t = 0.05 \text{ s}$	29
4.22 Acceleration of the numerical compound pendulum model using two-substep Newmark(0.6,0.5) method, $E = 1 \times 10^7 \text{ N/m}^2$, $\Delta t = 0.05 \text{ s}$	30
4.23 Acceleration of the numerical compound pendulum model using Bathe composite method, $E = 1 \times 10^7 \text{ N/m}^2$, $\Delta t = 0.05 \text{ s}$	30
4.24 Kinetic energy of the numerical compound pendulum model using two-substep Newmark(0.6,0.5) method, $E = 6 \times 10^{11} \text{ N/m}^2$, $\Delta t = 0.05 \text{ s}$. Straight reference line indicates initial potential energy.	31
4.25 Kinetic energy of the numerical compound pendulum model using Bathe composite method, $E = 6 \times 10^{11} \text{ N/m}^2$, $\Delta t = 0.05 \text{ s}$. Straight reference line indicates initial potential energy.	31
4.26 Kinetic energy of the numerical compound pendulum model using two-substep Newmark(0.6,0.5) method, $E = 1 \times 10^7 \text{ N/m}^2$, $\Delta t = 0.05 \text{ s}$. Straight reference line indicates initial potential energy.	32
4.27 Kinetic energy of the numerical compound pendulum model using Bathe composite method, $E = 1 \times 10^7 \text{ N/m}^2$, $\Delta t = 0.05 \text{ s}$. Straight reference line indicates initial potential energy.	32

4.28 Schema and description of the numerical cantilever beam model	33
4.29 Displacement of the numerical cantilever beam model using the trapezoidal rule, $\Delta t = 0.002s$	34
4.30 Velocity of the numerical cantilever beam model using the trapezoidal rule, $\Delta t = 0.002s$	35
4.31 Acceleration of the numerical cantilever beam model using the trapezoidal rule, $\Delta t = 0.002s$	35
4.32 Displacement of the numerical cantilever beam model using two-substep Newmark(0.5001,0.5) method, $\Delta t = 0.004s$	36
4.33 Displacement of the numerical cantilever beam model using two-substep Newmark(0.6,0.5) method, $\Delta t = 0.004s$	36
4.34 Displacement of the numerical cantilever beam model using Bathe composite method, $\Delta t = 0.004s$	37
4.35 Velocity of the numerical cantilever beam model using two-substep Newmark(0.5001,0.5) method, $\Delta t = 0.004s$	37
4.36 Velocity of the numerical cantilever beam model using two-substep Newmark(0.6,0.5) method, $\Delta t = 0.004s$	38
4.37 Velocity of the numerical cantilever beam model using Bathe composite method, $\Delta t = 0.004s$	38
4.38 Acceleration of the numerical cantilever beam model using two-substep Newmark(0.5001,0.5) method, $\Delta t = 0.004s$	39
4.39 Acceleration of the numerical cantilever beam model using two-substep Newmark(0.6,0.5) method, $\Delta t = 0.004s$	39
4.40 Acceleration of the numerical cantilever beam model using Bathe composite method, $\Delta t = 0.004s$	40
4.41 Schema and description of the numerical cylindrical shell model	41
4.42 Displacement of the numerical cylindrical shell model using the trapezoidal rule, $\Delta t = 0.0005s$	43
4.43 Displacement of the numerical cylindrical shell model using two-substep Newmark(0.6,0.5) method, $\Delta t = 0.001s$	43
4.44 Displacement of the numerical cylindrical shell model using two-substep Newmark(0.55,0.5) method, $\Delta t = 0.001s$	44

4.45 Displacement of the numerical cylindrical shell model using two-substep Newmark(0.55,0.55) method, $\Delta t = 0.001s$	44
4.46 Displacement of the numerical cylindrical shell model using Bathe composite method, $\Delta t = 0.001s$	45
A.1 Initial and current geometry of shell element	48



Chapter 1. Introduction

We deal with numerical error occur that occurs for nonlinear dynamics using the finite element method. This numerical error, often called nonlinear instability, has been studied by researchers who develop time integration methods. We present here the relationship between these three areas, and previous studies on time integration methods.

1.1 Finite element method in Nonlinear dynamics

Finite element method (FEM) has been the most successful technique of analyzing structures. Developments in FEM made it possible to analyze structures in a more realistic way, by including geometric or material nonlinearities which happens for the actual system. On the other hand, in order to add dynamic effect into this non-linear FEM, we cannot use mode-superposition because modes are changing at each step of non-linear analysis. Only possible method for non-linear dynamic analysis in FEM is to use time integration method. In time integration method, dynamic effects are included by velocity and acceleration calculated directly from the global displacement vector. Time integration method enables us to see the dynamic response including interaction of every mode in structure.

On the other hand, time integration method itself has two basic kinds: implicit and explicit. Strength of implicit method over explicit method is that we can use any kind of step size which guarantees analytical stability of response. Using the larger step size, response gets sparse in time domain and thus lose accuracy. However, in non-linear dynamics computation itself is often too costly that we want the response to be calculated using minimum number of step size. Because such cost-effectiveness could be achieved possibly by using implicit time integration method, it has been the reason of using implicit time integration in non-linear dynamics.

1.2 Nonlinear instability

Over many years, nature of numerical errors has been investigated. On the other hand, errors that occur during the analysis have been another concern because sometimes not enough information to determine the nature of the error. It is hard to decide, therefore, the most efficient way to suppress the error. This type of phenomenon has been widespread in the field of nonlinear dynamics, especially when high-frequency re-

sponse was tried to be calculated by using the trapezoidal rule. Because that the trapezoidal rule was the most accurate in the family of Newmark algorithm, researchers tended to modify the trapezoidal rule in developing new, error-stabilizing algorithms.

Instability of nonlinear dynamic analysis is dependent on time integration method. Park([1]) and Hughes([2]) were the earliest to discover instability of the trapezoidal rule. Many following researches on time integration field([1],[3-12]) was based on the motive that new time integration method is needed.

Instability of nonlinear dynamic analysis is also dependent on specific problems. Recent papers tended to deal with specific examples of nonlinear instability. Instability for large-displacement analysis of truss element([6],[8],[9],[12]), two-dimensional solid ([3],[6]), three-dimensional solid([10]), plate element([6]), and shell element([4],[11],[13]) were studied.

There was shift of focus from modifying time integration method into modifying element formulation([9],[11]). This change is along with the time integration method called Energy-Momentum Method or EMM([14]). EMM use geometry and strain of mid-configuration for calculation of the next configuration. This means in order to apply EMM, some modification on element level is inevitable. From that point, distinction between finite element formulation/time integration technologies has been blurred.

1.3 Implicit time integration methods

In order to solve nonlinear instabilities, many implicit time integration methods has been developed. Those studies can be classified into two major categories, methods with numerical damping and methods with average configuration. In fact, most of research papers devoted to time integration methods fall into category with numerical damping. In 1970's, based on the observation of Park, three-step method of Park([1]), HHT- α of Hilber([5]), and generalized- α of Chung([15]) were developed. Recently, Baig([3]) developed composite-time integration, Dong([10]) created BDF-like method, and Liu([6]) applied backward-Euler method on instability problems. On the other hand, papers related to average configuration are relatively small. Simo([11]), Kuhl([12]) and their co-workers studied the use of EMM, proposed by Simo([14]). However, Kuhl([4],[13]) observed convergence problem of EMM to create methods with numerical damping, CEMM and GEMM. Another major advantage of using numerical damping instead of average configuration is that no modification is required for the finite element. Similarly, we present a method which came the from parameter choice of classical Newmark method to be used just like method with numerical damping. Novel part of this method is that it does not use numerical damping, but just period elongation to solve instability problems. So far, no study was related to use of period elongation in solving instability, although the period elongation itself is a property common to all time integration methods. Further, we leave a room for a new time integration method including both period elongation and average configuration, or method that selectively encompasses period

elongation and numerical damping.



Chapter 2. General Theory

2.1 Non-linear formulation for structure

Formulation of non-linear dynamics is essentially based upon two things: non-linear formulation of structure and time integration method. To begin with, we review non-linear finite element formulation for static analysis.

Classically, there are two kinds of non-linear formulation of structure: Total Lagrangian and Updated Lagrangian formulation. The two formulations are analytically identical if relevant assumptions are used. However, our paper focuses on numerical instability which is not under control by analytic assumptions. Regarding this, many studies have been done implying it is better to use UL formulation than TL in dynamic analysis. We want to apologize that, on the other hand, due to subtleness of formulation in non-linear dynamics the numerical results in this paper were performed by finite element software ADINA V8.8. We explain the TL formulation as used in ADINA.

KAIST

2.1.1 Basic equation

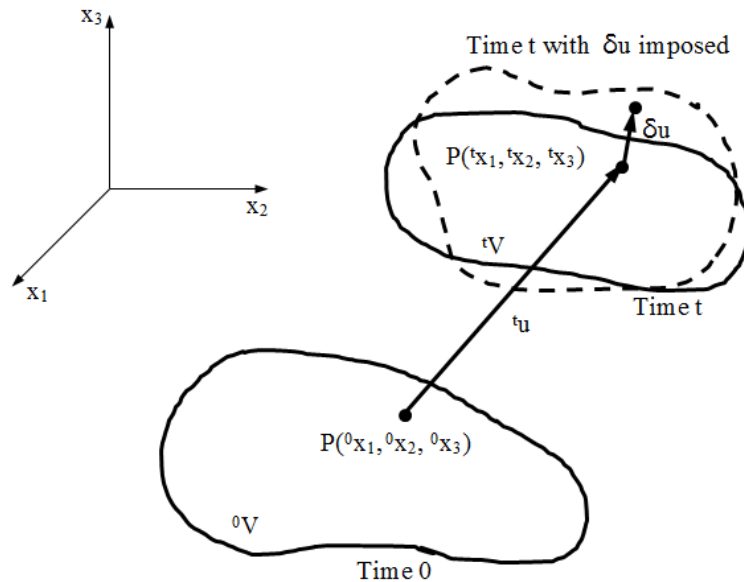


Figure 2.1. Initial and current geometry of body of a structure

Consider the structure with domain given in Fig. 2.1. Let us denote position of material particle P to be x_i with left superscript denote configuration. Displacement u_i at time t is written as,

$${}^t u_i = {}^t x_i - {}^0 x_i \quad (2.1)$$

Advantage of using TL over UL is we can use familiar strain measure, Green-Lagrange strain. Green-Lagrange strain tensor is defined as

$${}^t \underline{\underline{\varepsilon}} = \frac{1}{2} ({}^t \underline{\underline{X}}^T {}^t \underline{\underline{X}} - \underline{\underline{I}}) \quad (2.2)$$

$${}^t \underline{\underline{X}} = {}^t X_{ij} = \frac{\partial {}^t x_i}{\partial {}^0 x_j} \quad (2.3)$$

where ${}^t X_{ij}$ is deformation gradient and indices run from 1 to 3. This deformation gradient can be composed into rotational part ${}^t \underline{\underline{R}}$ and stretching part ${}^t \underline{\underline{U}}$,

$${}^t \underline{\underline{X}} = {}^t \underline{\underline{R}} {}^t \underline{\underline{U}} \quad (2.4)$$

where is ${}^t \underline{\underline{R}}$ an orthogonal matrix. Using this, it is easy to show that the Green-Lagrange strain is invariant under rigid-body rotation.

Before setting up an equilibrium equation, we want to find a stress measure where the work composed of the stress measure and Green-Lagrange strain is invariant under rigid-body rotation. Such known stress measure is second Piola-Kirchhoff stress, defined from physical Cauchy stress τ like below.

$${}^t S_{ij} = \frac{{}^0 \rho}{{}^t \rho} {}^t X_{ir} {}^t \tau_{rs} ({}^0 X^T)_{sj} = {}^t S = \frac{{}^0 \rho}{{}^t \rho} {}^t \underline{\underline{X}} {}^t \underline{\underline{\tau}} {}^0 \underline{\underline{X}}^T \quad (2.5)$$

where ρ is density of material point, ${}^0 X_{ij}$ is inverse of the deformation gradient ${}^t X_{ij}$ and indices run from 1 to 3. Important feature of this stress measure is that it is invariant under rigid-body rotation. Consider rigid body rotation R has occurred from configuration t to $t + \Delta t$ so that ${}^{t+\Delta t} \underline{\underline{x}} = \underline{\underline{R}} {}^t \underline{\underline{x}}$. Using transformation of second order tensor,

$${}^{t+\Delta t} \underline{\underline{\tau}} = \underline{\underline{R}} {}^t \underline{\underline{\tau}} \underline{\underline{R}}^T \quad (2.6)$$

and from transformation of geometry,

$${}^{t+\Delta t} \underline{\underline{X}} = \underline{\underline{R}} {}^t \underline{\underline{X}} \quad (2.7)$$

finally from physical consideration,

$${}^{t+\Delta t} \rho = {}^t \rho \quad (2.8)$$

From these it is easy to show that ${}^{t+\Delta t}{}_0S_{ij} = {}^t{}_0S_{ij}$.

On the other hand, Green-Lagrange strain in index form is,

$${}^t{}_0\varepsilon_{ij} = \frac{1}{2} \left(\frac{\partial^t x_k}{\partial^0 x_i} \frac{\partial^t x_k}{\partial^0 x_j} - \delta_{ij} \right) = \frac{1}{2} \left(\frac{\partial^t u_j}{\partial^0 x_i} + \frac{\partial^t u_i}{\partial^0 x_j} + \frac{\partial^t u_k}{\partial^0 x_i} \frac{\partial^t u_k}{\partial^0 x_j} \right) \quad (2.9)$$

This strain is often called separately as linear strain and nonlinear strain as in following equations.

$${}^t{}_0\varepsilon_{ij} = {}^t{}_0e_{ij} + {}^t{}_0\eta_{ij} \quad (2.10)$$

$${}^t{}_0e_{ij} = \frac{1}{2} \left(\frac{\partial^t u_j}{\partial^0 x_i} + \frac{\partial^t u_i}{\partial^0 x_j} \right) \quad (2.11)$$

$${}^t{}_0\eta_{ij} = \frac{1}{2} \left(\frac{\partial^t u_k}{\partial^0 x_i} \frac{\partial^t u_k}{\partial^0 x_j} \right) \quad (2.12)$$

In non-linear analysis, equilibrium equation must be set up in the current configuration. Otherwise, we cannot detect geometrical non-linearity arising from change in geometry during the analysis. For the body in Fig., we apply a virtual displacement field δu on the current configuration. By principle of virtual displacement, following equilibrium equation is obtained.

$$\int_V {}^t\tau_{ij} \delta {}^t e_{ij} dV = {}^tR \quad (2.13)$$

$$\delta {}^t e_{ij} = \frac{1}{2} \left(\frac{\partial \delta u_j}{\partial^t x_i} + \frac{\partial \delta u_i}{\partial^t x_j} \right) \quad (2.14)$$

Here tR is external load, is ${}^t\tau_{ij}$ physical Cauchy stress on current configuration, and $\delta {}^t e_{ij}$ is virtual linear strain produced by the applied virtual displacement. This virtual linear strain can be related to Green-Lagrange strain. If we take variation of (2.2),

$$\delta {}^t_0\varepsilon = \frac{1}{2} (\delta {}^t_0\underline{\underline{X}}^T {}^t_0\underline{\underline{X}} + {}^t_0\underline{\underline{X}}^T \delta {}^t_0\underline{\underline{X}}) \quad (2.15)$$

also note that

$$\delta {}^t_0\underline{\underline{X}}_{ij} = \delta \frac{\partial^t x_i}{\partial^0 x_j} = \frac{\partial \delta u_i}{\partial^0 x_j} = \frac{\partial \delta u_i}{\partial^t x_k} \frac{\partial^t x_k}{\partial^0 x_j} \quad (2.16)$$

which can be written in matrix form,

$$\delta {}^t_0\underline{\underline{X}} = \underline{\underline{\delta \mu}} {}^t_0\underline{\underline{X}} \quad (2.17)$$

$$\underline{\underline{\delta \mu}} = (\delta {}^t \mu)_{ij} = \frac{\partial \delta u_i}{\partial^t x_j} \quad (2.18)$$

Finally we relate the virtual linear strain in terms of virtual strain measure, or virtual Green-Lagrange strain.

$$\underline{\underline{\delta}}_0^t \underline{\underline{\varepsilon}} = {}^t \underline{\underline{X}}^T \frac{1}{2} ((\underline{\underline{\delta}}_t \underline{\underline{\mu}})^T + \underline{\underline{\delta}}_t \underline{\underline{\mu}}) {}^t \underline{\underline{X}} = {}^t \underline{\underline{X}}^T \underline{\underline{\delta}}_t e {}^t \underline{\underline{X}} \quad (2.19)$$

where $\underline{\underline{\delta}}_t e = \delta_t e_{ij}$ is the virtual linear strain.

(2.5) and (2.19) are rewritten using notation ${}^t x_{i,j} = \frac{\partial^t x_i}{\partial^0 x_j} = {}^t X_{ij}$ and substituted to (2.13),

$$\begin{aligned} \int_V {}^t \underline{\underline{\tau}} : \underline{\underline{\delta}}_t e d^t V &= \int_V \left(\frac{{}^t \rho}{\rho} {}^t S_{kl} {}^t x_{i,k} {}^t x_{j,l} \right) ({}^0 x_{m,i} {}^0 x_{n,j} \underline{\underline{\delta}}_0^t \varepsilon_{mn}) d^t V \\ &= \int_V \left(\frac{{}^t \rho}{\rho} {}^t S_{kl} \delta_{mk} \delta_{nl} \underline{\underline{\delta}}_0^t \varepsilon_{mn} \right) d^t V = \int_V {}^t S_{kl} \underline{\underline{\delta}}_0^t \varepsilon_{kl} d^0 V = \int_V {}^t \underline{\underline{S}} : \underline{\underline{\delta}}_0^t \underline{\underline{\varepsilon}} d^0 V \end{aligned} \quad (2.20)$$

We now distinguish the current configuration to be at time $t + \Delta t$, to distinguish the configuration at time t to be known configuration just before the current configuration. Finally, in TL formulation non-linear equilibrium equation is,

$$\int_V {}^{t+\Delta t} S_{ij} \delta^{t+\Delta t} \varepsilon_{ij} d^0 V = {}^{t+\Delta t} R \quad (2.21)$$

2.1.2 Linearization of basic equation

Having distinguished time t and time $t + \Delta t$ to be known and unknown configuration respectively, we need to use the known information into (2.21) and linearize it. First, we decompose displacement into known and unknown quantities.

$${}^{t+\Delta t} u_i = {}^t u_i + u_i \quad (2.22)$$

where u_i is called incremental displacement.

In each step, we must apply virtual displacement in lastly known configuration, in this case, time t . Therefore, virtual quantity of (2.22) reduces to

$$\delta^{t+\Delta t} u_i = \delta^t u_i + \delta u_i = \delta u_i \quad (2.23)$$

Using definition of (2.9) and (2.22), virtual Green-Lagrange strain is also written in terms of known and unknown quantities.

$${}^{t+\Delta t} \varepsilon_{ij} = {}^t \varepsilon_{ij} + {}_0 \varepsilon_{ij} \quad (2.24)$$

$${}_0\boldsymbol{\varepsilon}_{ij} = \frac{1}{2} \left(\frac{\partial u_j}{\partial^0 x_i} + \frac{\partial u_i}{\partial^0 x_j} + \frac{\partial_0^t u_k}{\partial^0 x_i} \frac{\partial u_k}{\partial^0 x_j} + \frac{\partial u_k}{\partial^0 x_i} \frac{\partial_0^t u_k}{\partial^0 x_j} + \frac{\partial u_k}{\partial^0 x_i} \frac{\partial u_k}{\partial^0 x_j} \right) \quad (2.25)$$

where ${}_0\boldsymbol{\varepsilon}_{ij}$ is called incremental Green-Lagrange strain. Taking virtual the quantity of (2.24) and using (2.23),

$$\delta^{t+\Delta t} {}_0\boldsymbol{\varepsilon}_{ij} = \delta_0^t \boldsymbol{\varepsilon}_{ij} + \delta_0 \boldsymbol{\varepsilon}_{ij} = \delta_0 \boldsymbol{\varepsilon}_{ij} \quad (2.26)$$

We can also think of decomposing the second Piola Kirchhoff stress.

$${}^{t+\Delta t} {}_0\boldsymbol{S}_{ij} = {}^t {}_0\boldsymbol{S}_{ij} + {}_0\boldsymbol{S}_{ij} \quad (2.27)$$

In this case, incremental second Piola-Kirchhoff stress ${}_0\boldsymbol{S}_{ij}$ is not related to other quantities. Here, we adopt linearization assumption.

$${}_0\boldsymbol{S}_{ij} = \left. \frac{\partial_0^t \boldsymbol{S}_{ij}}{\partial_0^t \boldsymbol{\varepsilon}_{rs}} \right|_t {}_0\boldsymbol{\varepsilon}_{rs} + \text{higher order terms} \doteq {}_0\boldsymbol{C}_{ijrs} {}_0\boldsymbol{\varepsilon}_{rs} \quad (2.28)$$

where we have assumed that value of $\frac{\partial_0^t \boldsymbol{S}_{ij}}{\partial_0^t \boldsymbol{\varepsilon}_{rs}}$ is constant throughout the whole configuration change.

This assumption of linear elastic material law on non-linear case is called St. Venant Kirchhoff material law. Putting (2.25), (2.26) and (2.27) into (2.21) we get linearized equilibrium equation,

$$\int_{{}_0V} {}_0\boldsymbol{C}_{ijrs} {}_0\boldsymbol{\varepsilon}_{rs} \delta_0 \boldsymbol{\varepsilon}_{ij} d^0V + \int_{{}_0V} {}^t \boldsymbol{S}_{ij} \delta_0 \boldsymbol{\varepsilon}_{ij} d^0V = {}^{t+\Delta t} \boldsymbol{R} \quad (2.29)$$

For computational purpose, we separate incremental strain (2.25),

$${}_0\boldsymbol{\varepsilon}_{ij} = {}_0\boldsymbol{e}_{ij} + {}_0\boldsymbol{\eta}_{ij} \quad (2.30)$$

$${}_0\boldsymbol{e}_{ij} = \frac{1}{2} \left(\frac{\partial u_j}{\partial^0 x_i} + \frac{\partial u_i}{\partial^0 x_j} + \frac{\partial_0^t u_k}{\partial^0 x_i} \frac{\partial u_k}{\partial^0 x_j} + \frac{\partial u_k}{\partial^0 x_i} \frac{\partial_0^t u_k}{\partial^0 x_j} \right) \quad (2.31)$$

$${}_0\boldsymbol{\eta}_{ij} = \frac{1}{2} \left(\frac{\partial u_k}{\partial^0 x_i} \frac{\partial u_k}{\partial^0 x_j} \right) \quad (2.32)$$

Quantity ${}_0\boldsymbol{e}_{ij}$ and ${}_0\boldsymbol{\eta}_{ij}$ are called incremental linear and non-linear strain respectively. ${}_0\boldsymbol{e}_{ij}$ represents linear part of incremental strain. We apply linearization to (2.29) once more,

$$\int_{{}_0V} {}_0\boldsymbol{C}_{ijrs} {}_0\boldsymbol{e}_{rs} \delta_0 \boldsymbol{e}_{ij} d^0V + \int_{{}_0V} {}^t \boldsymbol{S}_{ij} \delta_0 \boldsymbol{\eta}_{ij} d^0V = {}^{t+\Delta t} \boldsymbol{R} - \int_{{}_0V} {}^t \boldsymbol{S}_{ij} \delta_0 \boldsymbol{e}_{ij} d^0V \quad (2.33)$$

2.1.3 Linearized equation including dynamic effect

Consider a body force is included in the right-hand side of equilibrium equation (2.13). By principle of virtual displacement,

$$\int_{^tV} {}^t\tau_{ij} \delta {}^t e_{ij} d^tV = {}^tR + \int_{^tV} f_i \delta u_i d^tV \quad (2.34)$$

By D'Alembert's Principle, dynamic effect can be thought as a body force $f_i = -{}^t\rho^t \ddot{u}_i$ with density ρ and acceleration \ddot{u} . Substituting to (2.34),

$$\int_{^tV} {}^t\tau_{ij} \delta {}^t e_{ij} d^tV = {}^tR + \int_{^tV} -{}^t\rho^t \ddot{u}_i \delta u_i d^tV = {}^tR - \int_{^0V} {}^0\rho^t \ddot{u}_i \delta u_i d^0V \quad (2.35)$$

Making the current configuration as time $t + \Delta t$ and applying (2.35) to (2.33),

$$\int_{^0V} {}^0C_{ijrs} {}^0e_{rs} \delta {}^0e_{ij} d^0V + \int_{^0V} {}^0S_{ij} \delta {}^0\eta_{ij} d^0V = {}^{t+\Delta t}R - \int_{^0V} {}^0\rho^{t+\Delta t} \ddot{u}_i \delta u_i d^0V - \int_{^0V} {}^0S_{ij} \delta {}^0e_{ij} d^0V \quad (2.36)$$

In (2.36), virtual displacement $\delta \mathbf{u}$ is applied on the current configuration at time $t + \Delta t$.

2.2 Discretized equation and solution procedure

(2.36) can be discretized by using isoparametric interpolation procedure in finite element method.

That is, on the element domain of 0V_e ,

$$\underline{u}_e = \underline{H} \Delta U_e \quad (2.37)$$

$$\delta \underline{u}_e = \delta {}^{t+\Delta t} \underline{u}_e = \underline{H} \delta \Delta U_e = \underline{H} \delta U_e \quad (2.38)$$

$${}^{t+\Delta t} \underline{\ddot{u}}_e = \underline{H} {}^{t+\Delta t} \underline{\ddot{U}}_e \quad (2.39)$$

where \underline{U} is nodal displacement vector after assemblage and \underline{U}_e denote elemental nodal displacement vector. $\Delta \underline{U}$ is incremental nodal displacement, analogous to incremental displacement in (2.22). Using these displacement interpolation and definition (2.31) and (2.32), incremental strains are interpolated in a similar manner.

$${}^0\underline{e}_e = \underline{B}_L \Delta U_e \quad (2.40)$$

$$\delta {}^0\underline{\eta}_e = \delta U_e^T \underline{N}_{NL} \Delta U_e \quad (2.41)$$

Equilibrium equation (2.36) on element domain then becomes

$$\begin{aligned}
& \delta U_e^T \left[\int_{^0V_e} \underline{\underline{B}}_L^T \underline{\underline{C}} \underline{\underline{B}}_L d^0V_e + \int_{^0V} \underline{\underline{S}} : \underline{\underline{N}}_{NL} d^0V \right] \Delta U_e \\
& = {}^{t+\Delta t} R_e - \delta U_e^T \left[\int_{^0V_e} {}^0 \rho \underline{\underline{H}}^T \underline{\underline{H}} d^0V \right] {}^{t+\Delta t} \ddot{U}_e - \delta U_e^T \left[\int_{^0V_e} \underline{\underline{B}}_L^T \underline{\underline{S}} d^0V \right]
\end{aligned} \tag{2.42}$$

where material law $\underline{\underline{C}}$ and stresses $\underline{\underline{S}}$ and $\underline{\underline{S}}$ are appropriately defined. We can assemble the element domains 0V_e into global domain 0V . Regarding external force as external virtual work and canceling the virtual quantities, final discretized equilibrium equation in matrix form is,

$$\underline{\underline{M}} {}^{t+\Delta t} \ddot{U} + (\underline{\underline{K}}_L + \underline{\underline{K}}_{NL}) \Delta U = {}^{t+\Delta t} R - \underline{\underline{F}} \tag{2.43}$$

$$\underline{\underline{K}}_L({}^{t+\Delta t} U) = \sum_e \int_{^0V_e} \underline{\underline{B}}_L^T \underline{\underline{C}} \underline{\underline{B}}_L d^0V \tag{2.44}$$

$$\underline{\underline{K}}_{NL}({}^{t+\Delta t} U) = \sum_e \int_{^0V} \underline{\underline{B}}_{NL}^T \underline{\underline{S}} \underline{\underline{B}}_{NL} d^0V \tag{2.45}$$

$$\underline{\underline{M}} = \sum_e \int_{^0V_e} {}^0 \rho \underline{\underline{H}}^T \underline{\underline{H}} d^0V \tag{2.46}$$

$$\underline{\underline{F}}({}^{t+\Delta t} U) = \sum_e \int_{^0V_e} \underline{\underline{B}}_L^T \underline{\underline{S}} d^0V \tag{2.47}$$

Parenthesis in (2.44), (2.45) and (2.47) indicates that the entries are function of current displacement. To illustrate its usage, we discuss in Appendix the forms of the matrices used in (2.42) for four-node shell element.

Chapter 3. Time Integration Methods

3.1 Newmark time integration method

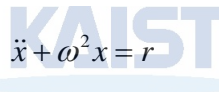
In (2.43), we did not have information about ${}^{t+\Delta t}\ddot{U}$. We wish to solve (2.43) in terms of ${}^{t+\Delta t}U$ only, and method required for doing so is time integration method.

Basic equation of Newmark time integration ([16]) is the following two assumptions.

$${}^{t+\Delta t}U = {}^tU + {}^t\dot{U}\Delta t + (1 - \beta_0){}^t\ddot{U}\frac{\Delta t^2}{2} + \beta_0{}^{t+\Delta t}\ddot{U}\frac{\Delta t^2}{2} \quad (3.1)$$

$${}^{t+\Delta t}\dot{U} = {}^t\dot{U} + (1 - \beta_1){}^t\ddot{U}\Delta t + \beta_1{}^{t+\Delta t}\ddot{U}\Delta t \quad (3.2)$$

Newmark time integration has two parameters of β_0 and β_1 , which we would preferably call Newmark(β_0, β_1). These two parameters play important role in changing error characteristic of Newmark time integration method, as discussed next.



$$\ddot{x} + \omega^2 x = r \quad (3.3)$$

Any time integration methods have inherent analytical error. Depending on the discretization and frequency of structure, time integration methods exhibits two types of error, amplitude decay and period elongation. The two errors literally means what happens for homogeneous solution of (3.3) was analyzed by any time integration method. (3.3) is one-degree-of-freedom system with displacement x , frequency ω , where r is excitation due to external load or initial conditions. To apply implicit time integration method, equilibrium equation of (3.3) is discretized for the current step.

$${}^{t+\Delta t}\ddot{x} + \omega^2{}^{t+\Delta t}x = {}^{t+\Delta t}r \quad (3.4)$$

In order to see inherent error of using time integration for the discretized equilibrium equation, we attempt to extract characteristic of homogeneous solution. As in [5], [17] and [18], (3.1), (3.2) and (3.4) can be rearranged in the following form.

$$\begin{bmatrix} {}^{t+\Delta t}\ddot{x} \\ {}^{t+\Delta t}\dot{x} \\ {}^{t+\Delta t}x \end{bmatrix} = \underline{\underline{A}} \begin{bmatrix} {}^t\ddot{x} \\ {}^t\dot{x} \\ {}^tx \end{bmatrix} + \underline{L} \quad (3.5)$$

In (3.4), responses in the next step are determined by those of previous step, with multiplication by matrix A and addition with vector L. It is the matrix A which contains the information about the two types of

error. This matrix is called amplification matrix, and for the Newmark method following form is obtained.

$$\underline{\underline{A}} = \begin{bmatrix} -(\frac{1}{2} - \frac{1}{2}\beta_0)\chi & \frac{1}{\Delta t}(-\chi) & \frac{1}{\Delta t^2}(-\chi) \\ \Delta t(1 - \beta_1 - (\frac{1}{2} - \frac{1}{2}\beta_0)\beta_1\chi) & 1 - \chi\beta_1 & \frac{1}{\Delta t}(-\chi\beta_1) \\ \Delta t^2(\frac{1}{2} - \frac{1}{2}\beta_0)(1 - \frac{1}{2}\beta_0\chi) & \Delta t(1 - \frac{1}{2}\beta_0\chi) & 1 - \frac{1}{2}\beta_0\chi \end{bmatrix} \quad (3.6)$$

$$\chi = (\frac{1}{\omega^2\Delta t^2} + \frac{1}{2}\beta_0)^{-1} \quad (3.7)$$

(3.6) has three eigenvalues, one zero eigenvalue and two complex conjugate ones. Amplitude error can be investigated from absolute value of maximum eigenvalue of (3.6), which is given by the following equation, (3.8).

$$\begin{aligned} \rho(A) &\equiv |\max .eigenvalue\ of\ A| \\ &= (T^2 + 2\beta_0\Delta t^2\pi^2)^{-1} |(2\beta_0\Delta t^2\pi^2 - \Delta t^2\pi^2 + T^2 - 2\beta_1\Delta t^2\pi^2) \\ &\quad + I \cdot \sqrt{\Delta t^2\pi^2(8\beta_0\Delta t^2\pi^2 - \Delta t^2\pi^2 + 4T^2 - 4\beta_1\Delta t^2\pi^2 - 4\beta_1^2\Delta t^2\pi^2)}| \end{aligned} \quad (3.8)$$

$$T = \frac{2\pi}{\omega} \quad (3.9)$$

This value is called spectral radius of Newmark time integration method. This value can be plotted with a range of non-dimensional frequency $\Delta t/T$, where T is period which is related to frequency ω by (3.9). Since given analytical amplitude of response is 1.0, spectral radius less than 1.0 means amplitude error occurs. On the other hand, if the spectral radius is greater than 1.0 response become magnified at each step until it diverge. Therefore, spectral radius must be less than or equal to 1.0 to insure analytical stability of analysis.

Calculated period is also not the same to analytical period T . Calculated frequency $\bar{\omega}$ is related to phase of maximum eigenvalue of (3.5) Ω by,

$$\bar{\omega} = \frac{\Omega}{\Delta t} \quad (3.10)$$

$$\begin{aligned} \Omega &= \arctan\left(\frac{\sqrt{\Delta t^2\pi^2(8\beta_0\Delta t^2\pi^2 - \Delta t^2\pi^2 + 4T^2 - 4\beta_1\Delta t^2\pi^2 - 4\beta_1^2\Delta t^2\pi^2)}}{(2\beta_0\Delta t^2\pi^2 - \Delta t^2\pi^2 + T^2 - 2\beta_1\Delta t^2\pi^2)}\right) \end{aligned} \quad (3.11)$$

From this, calculated period \bar{T} is given and relative period elongation can be constructed, which is also a function of non-dimensional frequency.

$$period\ elongation \equiv \frac{\bar{T} - T}{T} \quad (3.12)$$

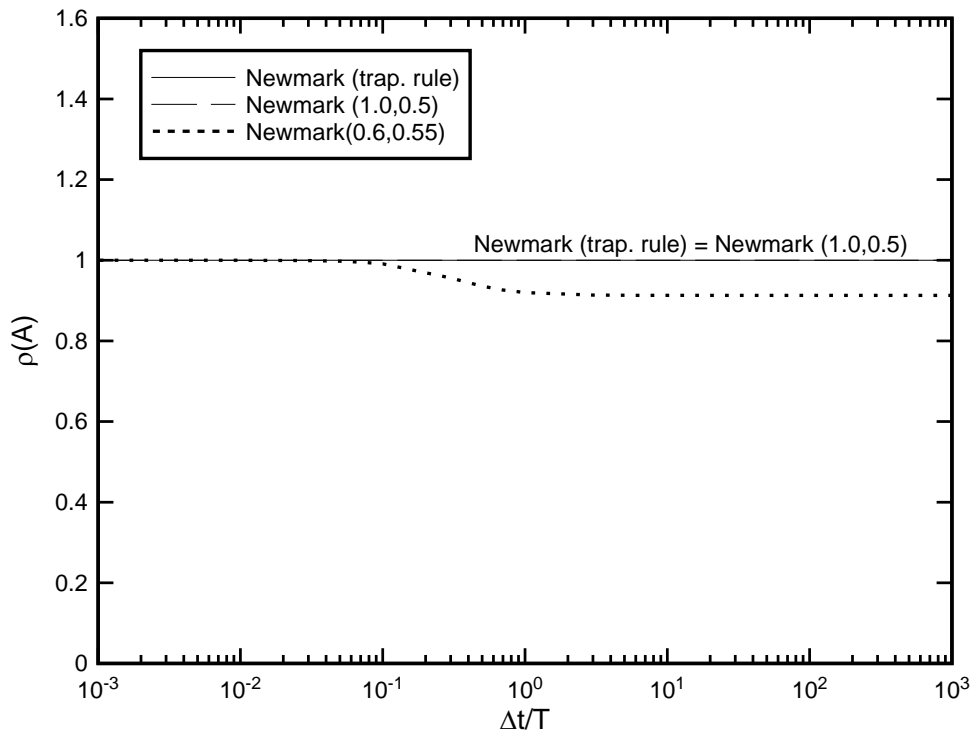


Figure 3.1. Spectral radius of Newmark method

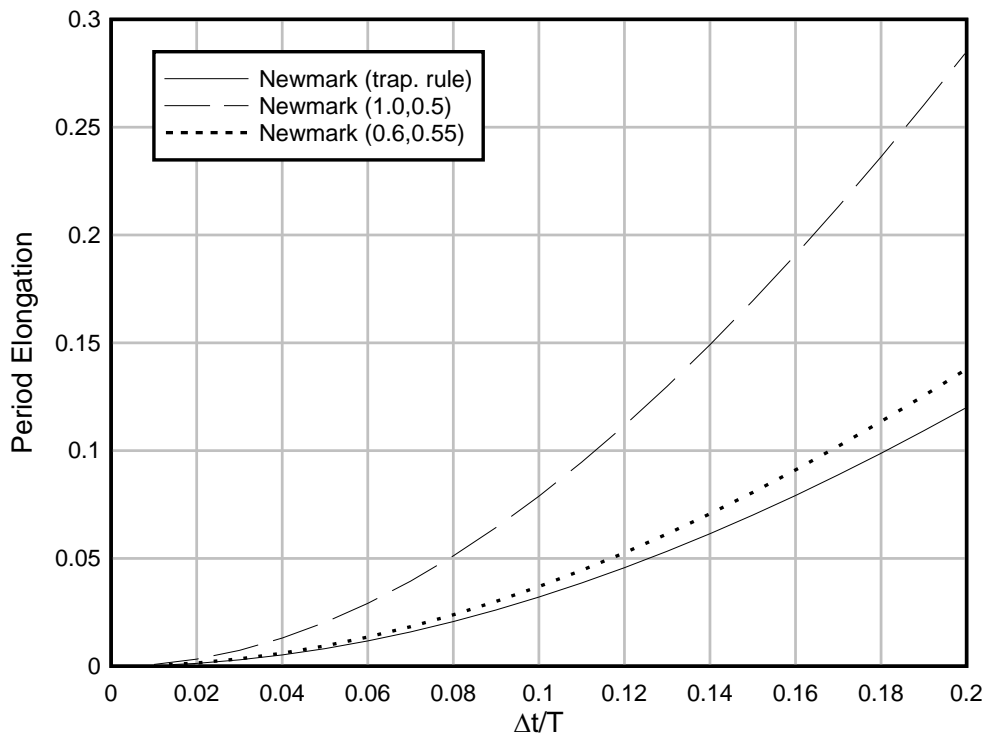


Figure 3.2. Period elongation of Newmark method

$$\bar{T} = \frac{2\pi}{\omega} \quad (3.13)$$

Spectral radius and period elongation for various parameter of Newmark method is shown in Fig. 3.1 and Fig. 3.2. Choice of parameter Newmark(0.5,0.5) is called the trapezoidal rule.

On the other hand, value of spectral radius less than 1.0 for high values of non-dimensional frequency has been a desirable characteristic for time integration methods, because it can prevent nonlinear instability. If value of spectral radius is less than 1.0, given time integration method is referred as ‘method with numerical damping’ and this characteristic is itself called numerical damping.

Larger value of parameter β_1 increases numerical damping, while larger value of parameter β_0 increases period elongation. These distinctive parameters are main characteristic of Newmark method. If $\beta_1 = \frac{1}{2}$, parameter β_0 is independent of numerical damping, but it introduce more period elongation. This parameter choice, i.e. increase of β_0 with $\beta_1 = \frac{1}{2}$, is of significant importance because we can decouple and apply only the period elongation.

3.2 Bathe composite time integration method

Many methods related to numerical damping have been studied. Many of them have parameters to introduce numerical damping or additional constraints which naturally result in numerical damping. Bathe composite method([7],[8]) is one of them, and numerical damping is introduced with three-point backward difference formula applied at the second sub-step. We describe this process in detail.

Basically, like other ‘composite’ methods, Bathe composite method uses sub-step. It means that for a given value of Δt we actually use $\frac{\Delta t}{n}$, perform n times the computation than the original method, and use only the finally computed values as responses. Bathe composite method is a two-substep method, and for the first sub-step it uses the trapezoidal rule.

$${}^{t+\frac{\Delta t}{2}}U = {}^tU + {}^t\dot{U}(\Delta t/2) + {}^t\ddot{U} \frac{(\Delta t/2)^2}{4} + {}^{t+\frac{\Delta t}{2}}\ddot{U} \frac{(\Delta t/2)^2}{4} \quad (3.14)$$

$${}^{t+\frac{\Delta t}{2}}\dot{U} = {}^t\dot{U} + \frac{1}{2}{}^t\ddot{U}(\Delta t/2) + \frac{1}{2}{}^{t+\frac{\Delta t}{2}}\ddot{U}(\Delta t/2) \quad (3.15)$$

For the second sub-step, three-point backward difference formula is applied to velocity and acceleration, replacing the two original assumptions.

$${}^{t+\Delta t}\ddot{U} = c_1\dot{U} + c_2{}^{t+\frac{\Delta t}{2}}\dot{U} + c_3{}^{t+\Delta t}\dot{U} \quad (3.16)$$

$${}^{t+\Delta t}\dot{U} = c_1U + c_2{}^{t+\frac{\Delta t}{2}}U + c_3{}^{t+\Delta t}U \quad (3.17)$$

.where constants are given by

$$c_1 = \frac{1-\gamma}{\Delta t \gamma}, \quad c_2 = \frac{-1}{(1-\gamma)\gamma \Delta t}, \quad c_3 = \frac{2-\gamma}{(1-\gamma)\Delta t} \quad (3.18)$$

With normal splitting of time step, i.e. using $\frac{\Delta t}{2}$ for the first sub-step, $\gamma = 0.5$ performs well, as described in [7].

In addition, any method can be made as sub-step method. Normally if we do not have additional multi-step constraint like (3.16) and (3.17), we do not make an algorithm sub-step. In this paper, however, Newmark method was made as two-substep method in order to equalize computational cost with the Bathe composite method.

3.3 Solution procedure

We solve (2.43) in terms of incremental displacement, updating the current displacement, velocity and acceleration. However, right-hand-side of (2.43) has unknown, as (2.47) is unknown and changing. Therefore, we solve iteratively with the updates of (2.44), (2.45) and (2.47). This process is on Table 3.1.

Table 3.1. Computational process for equilibrium

Given the current step $t + \Delta t$,	
assume for initial iteration ${}^{t+\Delta t}U^{(1)} = {}^tU^{(last\ iteration)}$ and ${}^{t+\Delta t}\underline{F}^{(1)} = {}^t\underline{F}^{(last\ iteration)}$	
Iterate for $i = 1, 2, \dots$	Solve (2.43) with time integration assumption ((3.1); (3.14); (3.16)) to obtain ΔU If right-hand-side of (2.42) is under tolerance of (3.18), exit.
	Update ${}^{t+\Delta t}U^{(i)} = {}^{t+\Delta t}U^{(i-1)} + \Delta U$ Update (2.44), (2.45), (2.47) Update ${}^{t+\Delta t}\dot{U}, {}^{t+\Delta t}\ddot{U}$ using time integration assumptions ((3.1) and (3.2); (3.14) and (3.15); (3.16) and (3.17))

Notice that as equilibrium is met, both sides of (2.43) gets smaller and smaller. Thus, we can stop the solution process with giving small tolerance to right-hand-side of (2.43). ADINA use energy tolerance,

$$\frac{\Delta U^{(i)T} (RHS^{(i)})}{\Delta U^{(1)T} (RHS^{(1)})} \leq etol \quad (3.18)$$

where $etol = 10^{-3}$ is given as default. Process in Table 3.1 is full Newton-Raphson iteration since left-

hand-side of equilibrium, (2.44) and (2.45), are updated after each iteration.

3.4 Other methods

There are other important time integration method, Midpoint rule([11],[12]) and Energy-Momentum Method([4],[11],[12],[13],[14]). Reason we are giving here is they are sensitive to entire formulation and solution process. We had no chance to rigorously formulate those methods. According to [12], both methods use following equilibrium.

$$\underline{\underline{M}}^{t+\frac{\Delta t}{2}} \ddot{\underline{U}} + (\underline{\underline{K}}_{L,\frac{1}{2}} + \underline{\underline{K}}_{NL,\frac{1}{2}}) \Delta U = {}^{t+\Delta t}R - \underline{F}_{\frac{1}{2}} \quad (3.19)$$

We only discuss difference in (2.46). Midpoint rule use following internal force.

$$\underline{F}_{\frac{1}{2}}({}^{t+\Delta t}U) = \sum_e \int_{{}^0V_e} (\underline{\underline{B}}_L(\frac{1}{2}({}^{t+\Delta t}U + {}^tU)))^T \underline{S}(\frac{1}{2}({}^{t+\Delta t}U + {}^tU)) d^0V \quad (3.20)$$

Parentheses after $\underline{F}_{\frac{1}{2}}$, $\underline{\underline{B}}_L$ and \underline{S} indicate dependence to displacement. Notice that we use mid-point equilibrium and matrices computed via mid-point displacements. For Energy-Momentum Method, internal force is different with mid-point rule.

$$\underline{F}_{\frac{1}{2}}({}^{t+\Delta t}U) = \sum_e \int_{{}^0V_e} (\underline{\underline{B}}_L(\frac{1}{2}({}^{t+\Delta t}U + {}^tU)))^T \frac{1}{2}(\underline{S}({}^{t+\Delta t}U) + \underline{S}({}^tU)) d^0V \quad (3.21)$$

In this case, stresses are averaged instead of displacements.

Chapter 4. Numerical Results

4.1 Rotating pendulum

We solve rotating pendulum problem in [8]. Schema and description of numerical rotating pendulum model is shown in Fig. 4.1. It is modeled with single two-node truss (rod or bar) element. The model is subjected with no external loading except for initial conditions. Initial velocity drives the rotating pendulum and initial acceleration was applied for canceling out centrifugal acceleration at the tip.

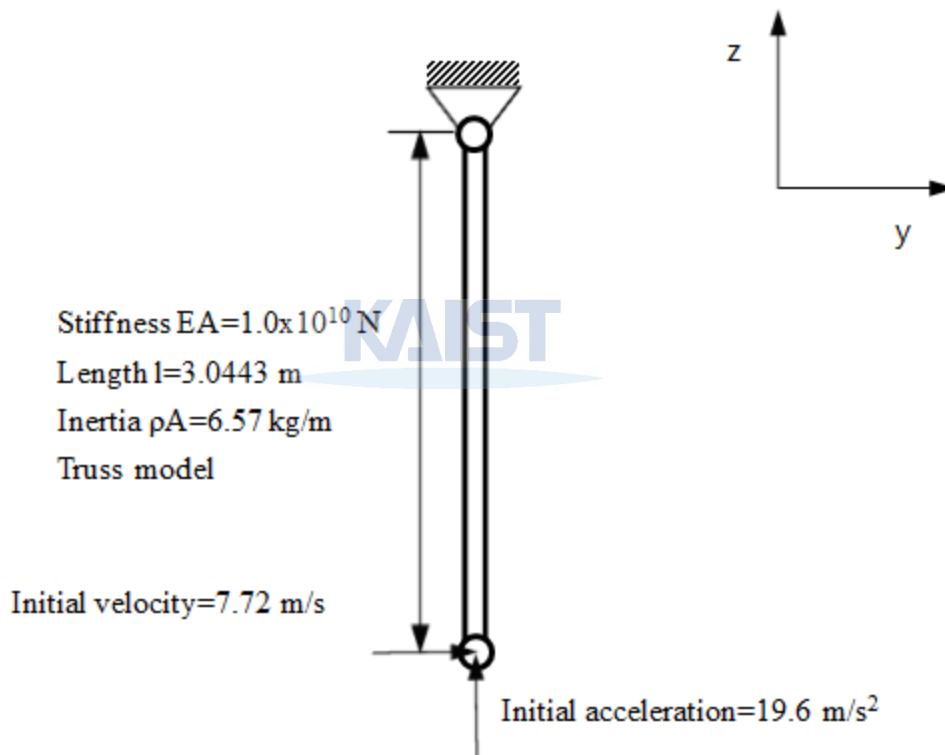


Figure 4.1. Schema and description of the numerical rotating pendulum model

Table 4.1. Choice of parameter of numerical rotating pendulum for the evaluation of performance

Method	Parameter	Step size (Δt)	Stiffness (EA)
The trapezoidal rule	-	0.01s	$10^{10} N$
Two-substep Newmark	(0.6,0.5)	0.5s	$10^3 N$ and $10^{10} N$
Bathe composite	-	0.5s	$10^3 N$ and $10^{10} N$

For the trapezoidal rule, small step size and default stiffness was selected for the demonstration of instability. Because use of small step size with candidate methods give almost exact solution for this problem, response using the larger step size was demonstrated for comparison of the candidate methods. Because dominant global response, a low-frequency motion of rigid-body rotation of rotating pendulum, is depending on density and initial velocity and not on stiffness, stiffness was changed to observe variety of solutions.

Fig. 4.2 to 4.11 shows velocity and acceleration of the methods in Table 4.1.

When the trapezoidal rule is used, velocity and kinetic energy are conserved exactly until continuous accumulation of acceleration stops the solution. On the other hand, two-substep Newmark(0.6,0.5) and Bathe composite method remains converged even for the larger step size and variety of stiffness.

Unlike Bathe composite method, two-substep Newmark(0.6,0.5) showed almost no decay of velocity in stiffness $10^{10} N$. Strength and weakness of those two candidate methods can be compared for the case of stiffness $10^3 N$. This case also shows that two-substep Newmark(0.6,0.5) has better conservation of velocity, but smoothness of accuracy is better for Bathe composite method. In the next example, these differences are demonstrated in a more dramatic manner.

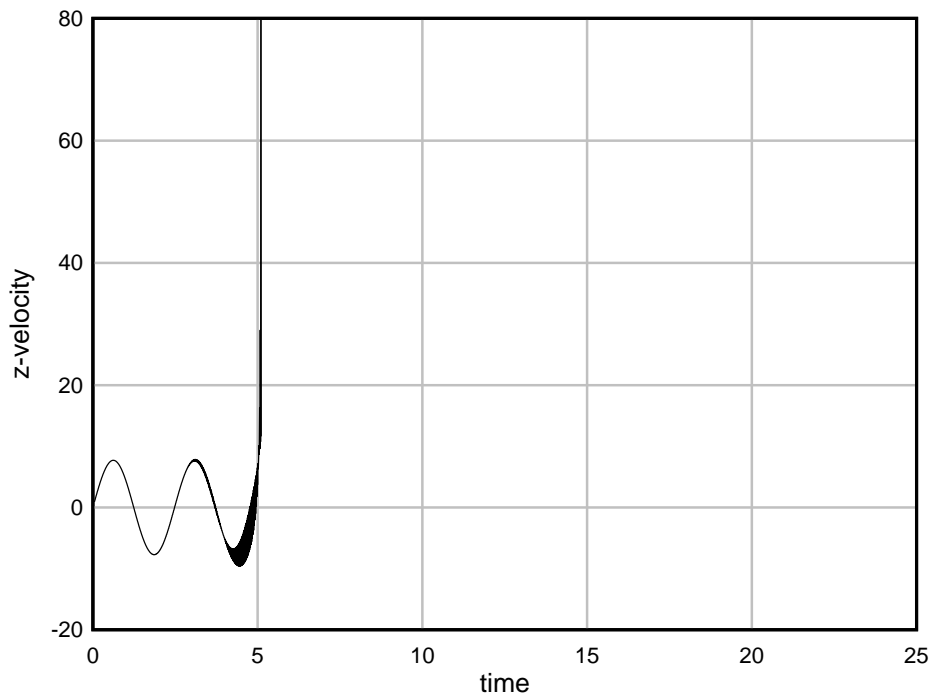


Figure 4.2. Velocity of the numerical rotating pendulum model using the trapezoidal

rule, $EA = 10^{10} N$, $\Delta t = 0.01s$

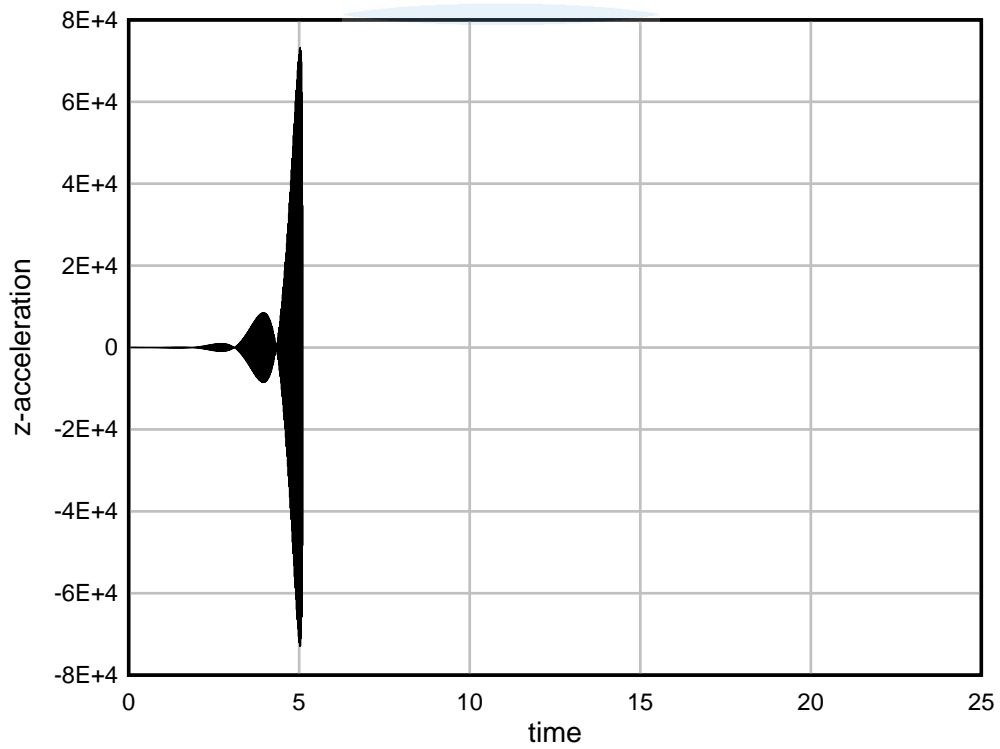


Figure 4.3. Acceleration of the numerical rotating pendulum model using the trapezoidal rule, $EA = 10^{10} N$,

$\Delta t = 0.01s$

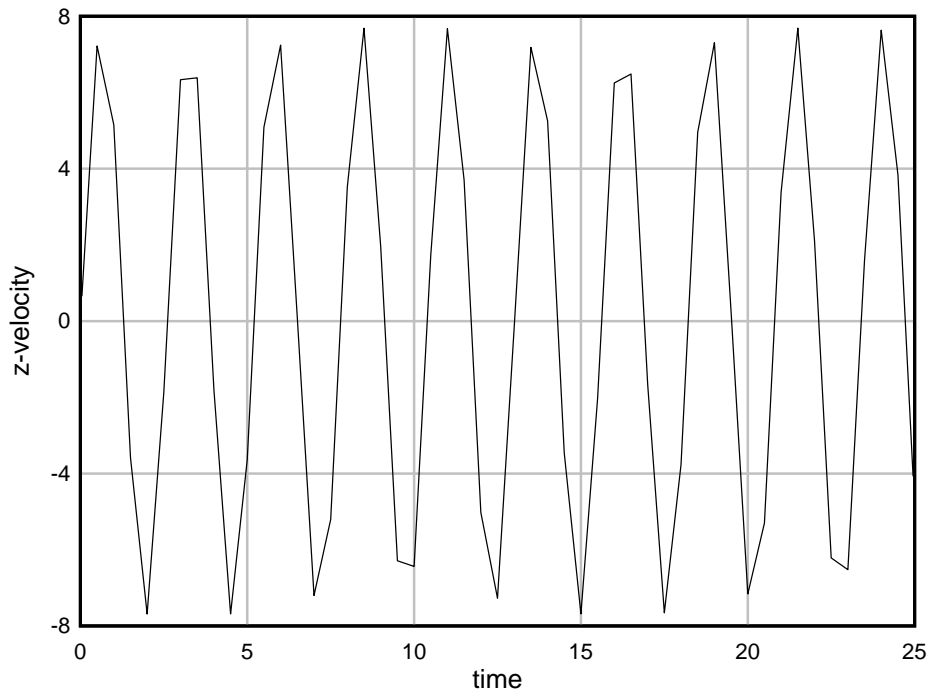


Figure 4.4. Velocity of the numerical rotating pendulum model using two-substep Newmark(0.6,0.5) method,

$$EA = 10^{10} N, \Delta t = 0.5 s$$

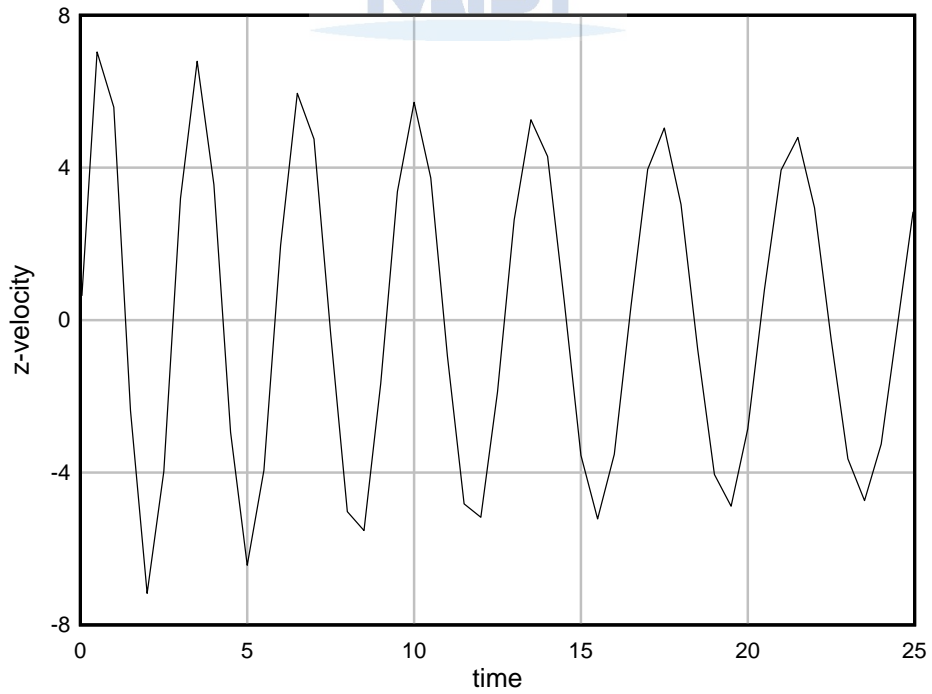


Figure 4.5. Velocity of the numerical rotating pendulum model using Bathe composite method, $EA = 10^{10} N$,

$$\Delta t = 0.5 s$$

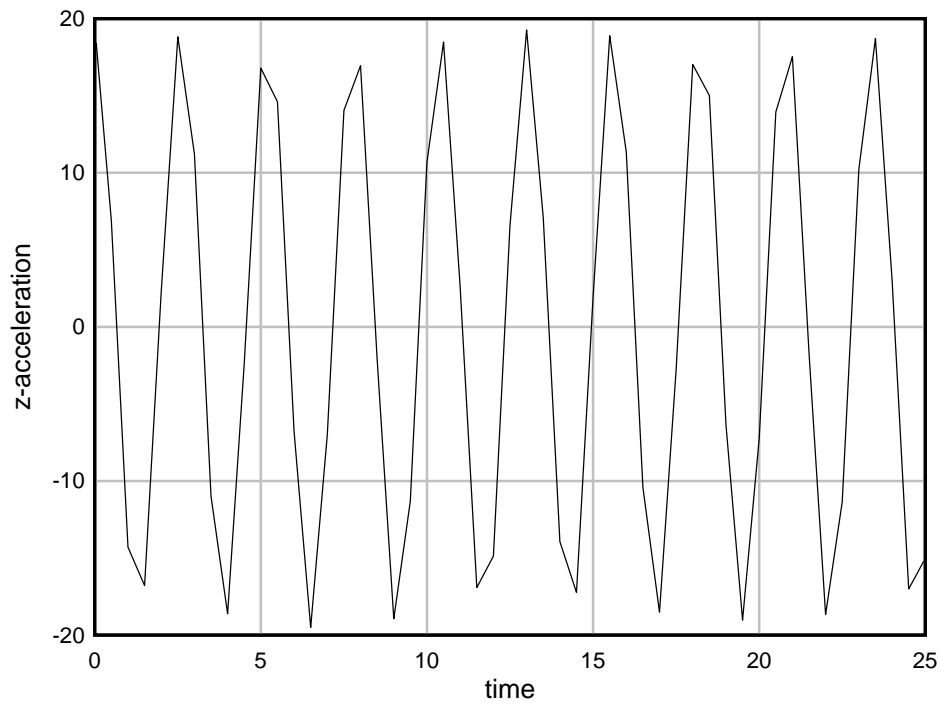


Figure 4.6. Acceleration of the numerical rotating pendulum model using two-substep Newmark(0.6,0.5) method, $EA = 10^{10} N$, $\Delta t = 0.5 s$

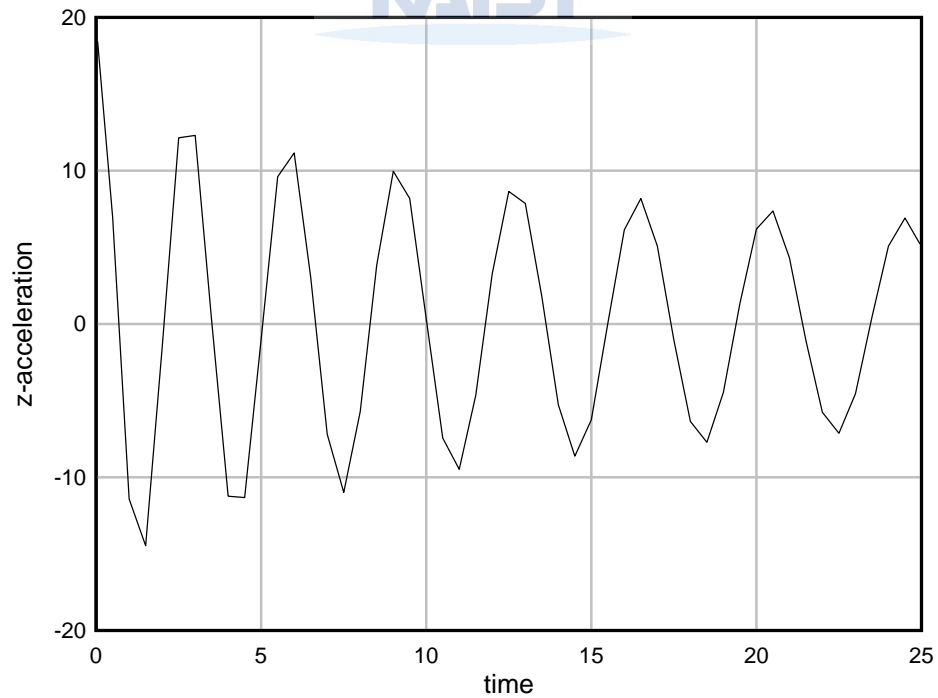


Figure 4.7. Acceleration of the numerical rotating pendulum model using Bathe composite method, $EA = 10^{10} N$, $\Delta t = 0.5 s$

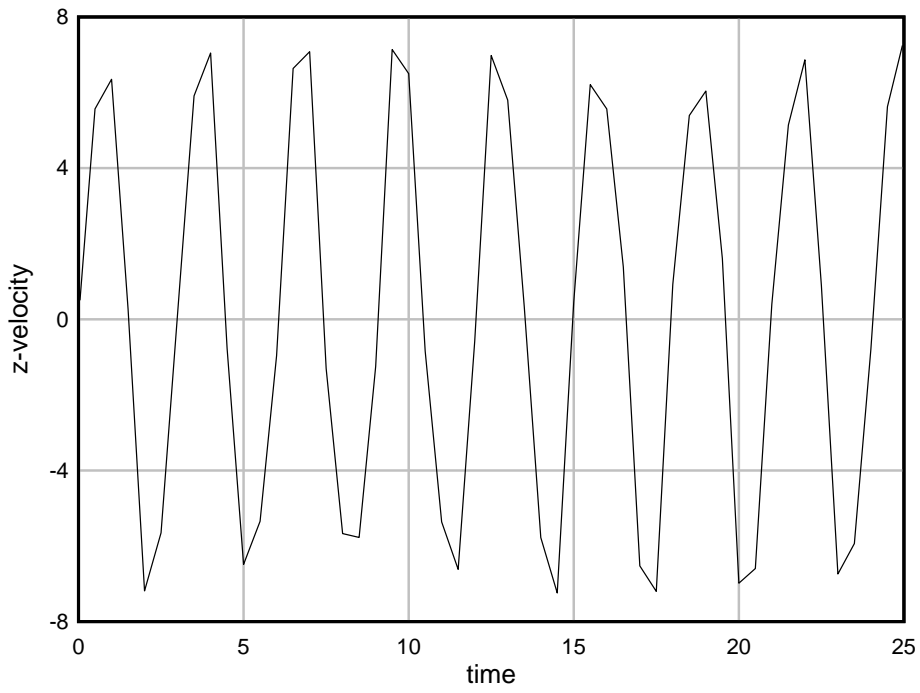


Figure 4.8. Velocity of the numerical rotating pendulum model using two-substep Newmark(0.6,0.5) method,

$$EA = 10^3 N, \Delta t = 0.5 s$$

KAIST

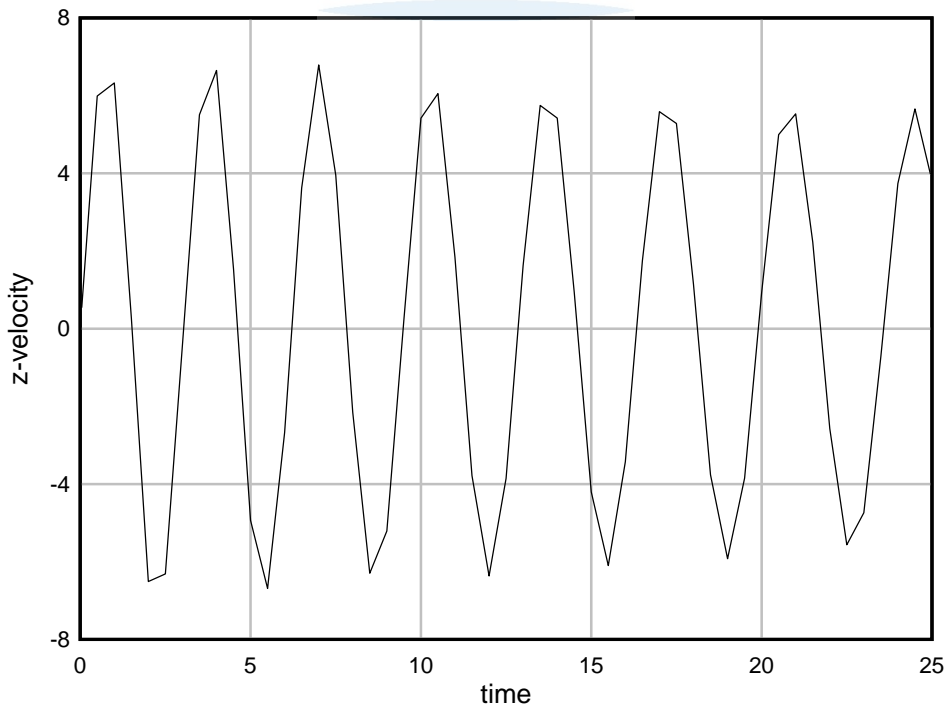


Figure 4.9. Velocity of the numerical rotating pendulum model using Bathe composite method, $EA = 10^3 N$,

$$\Delta t = 0.5 s$$

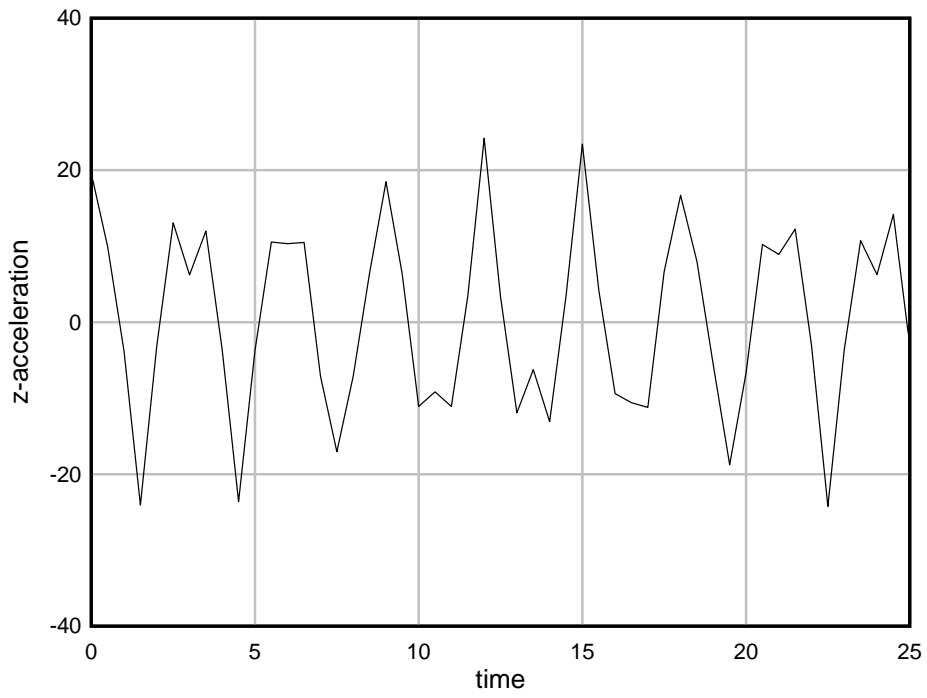


Figure 4.10. Acceleration of the numerical rotating pendulum model using two-substep Newmark(0.6,0.5) method, $EA=10^3 N$, $\Delta t = 0.5 s$

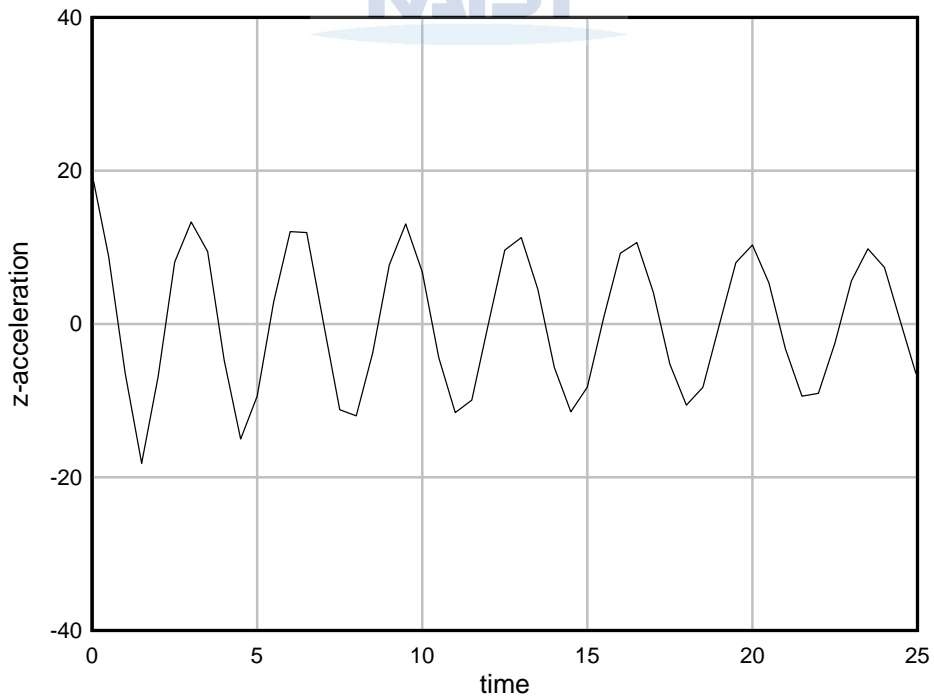


Figure 4.11. Acceleration of the numerical rotating pendulum model using Bathe composite method, $EA=10^3 N$, $\Delta t = 0.5 s$

4.2 Compound pendulum

We solve compound pendulum in [7]. It is modeled with 40 four-node two-dimensional solid elements, two elements in the thickness direction and 20 elements in the longitudinal direction. The model is subjected to mass-proportional loading of gravity, which gives initial potential energy for the motion of the compound pendulum.

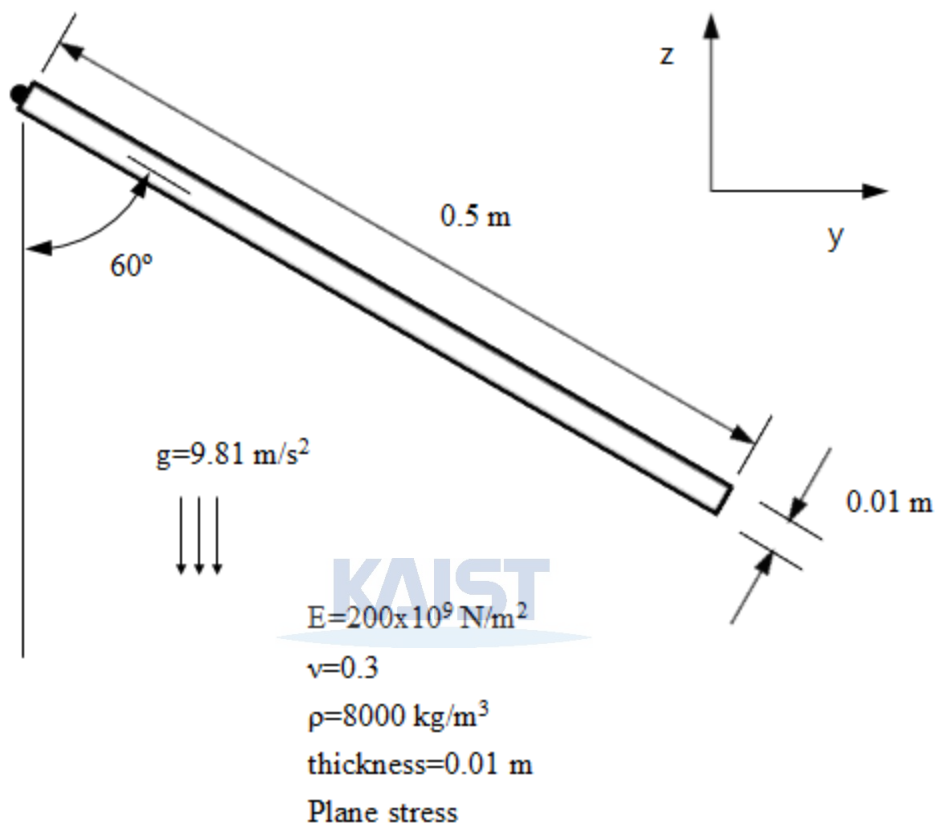


Figure 4.12. Schema and description of the numerical compound pendulum model

Table 4.2. Choice of parameter of numerical compound pendulum for the evaluation of performance

Method	Parameter	Step size (Δt)	Stiffness (E)
The trapezoidal rule	-	0.005 s	$2 \times 10^{11} \text{ N/m}^2$
Two-substep Newmark	(0.6,0.5)	0.05 s	$1 \times 10^7 \text{ N/m}^2$ and $6 \times 10^{11} \text{ N/m}^2$
Bathe composite	-	0.05 s	$1 \times 10^7 \text{ N/m}^2$ and $6 \times 10^{11} \text{ N/m}^2$

As in the literature, the trapezoidal rule was used to show instability of the numerical compound pendulum model. Again, use of small step size with candidate methods give almost exact solution for this problem, response using the larger step size was demonstrated for comparison of the candidate methods. Because dominant global response, a low-frequency motion of rigid-body swing of compound pendulum, is depending

on density and gravity and not on stiffness, stiffness was changed to observe variety of solutions.

Fig. 4.13 to 4.27 shows velocity, acceleration and kinetic energy of the methods in Table 4.2.

When the trapezoidal rule is used, velocity and kinetic energy are conserved exactly until continuous accumulation of acceleration stops the solution. On the other hand, two-substep Newmark(0.6,0.5) and Bathe composite method remains converged even for the larger step size and variety of stiffness.

One difference between two-substep Newmark(0.6,0.5) and Bathe composite is degree of conservation of amplitude of velocity and kinetic energy. In this problem, two-substep Newmark(0.6,0.5) conserved those quantities better than Bathe composite method. It means for this problem, period elongation performs better than amplitude decay (numerical damping) in terms of conservation. On the other hand, one weakness of two-substep Newmark(0.6,0.5) is revealed via acceleration. For stiffness of $1 \times 10^7 N/m^2$, two-substep Newmark(0.6,0.5) have spurious high-frequency response as like the trapezoidal rule demonstrated in the other literature [17] for simpler ODE problem. Thus, two-substep Newmark(0.6,0.5) should be used for the problems where conservation of velocity and kinetic energy is more important than response of acceleration itself.

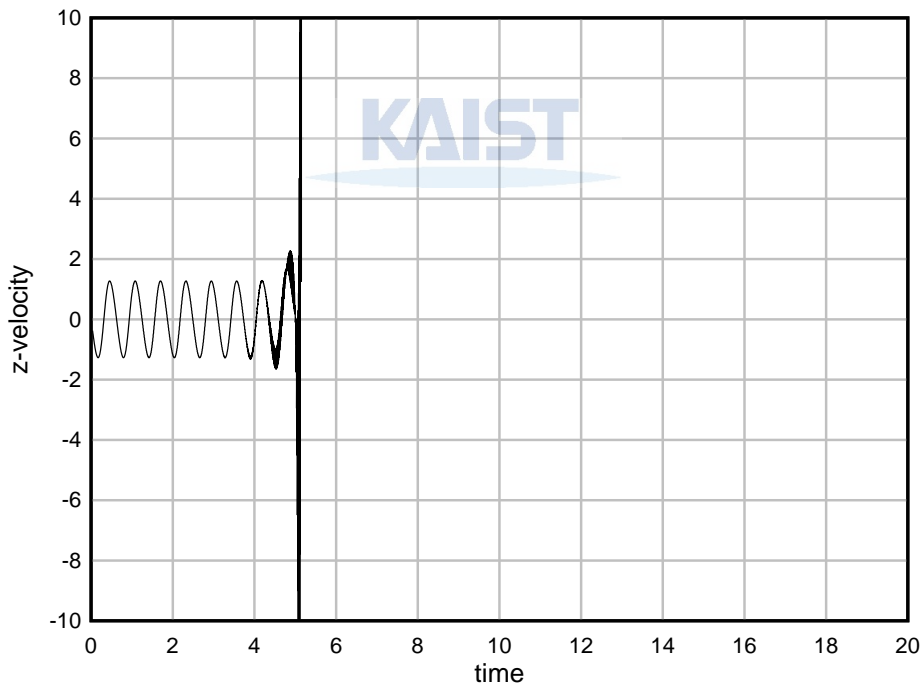


Figure 4.13. Velocity of the numerical compound pendulum model using the trapezoidal rule,

$$E = 2 \times 10^{11} N/m^2, \Delta t = 0.005 s$$

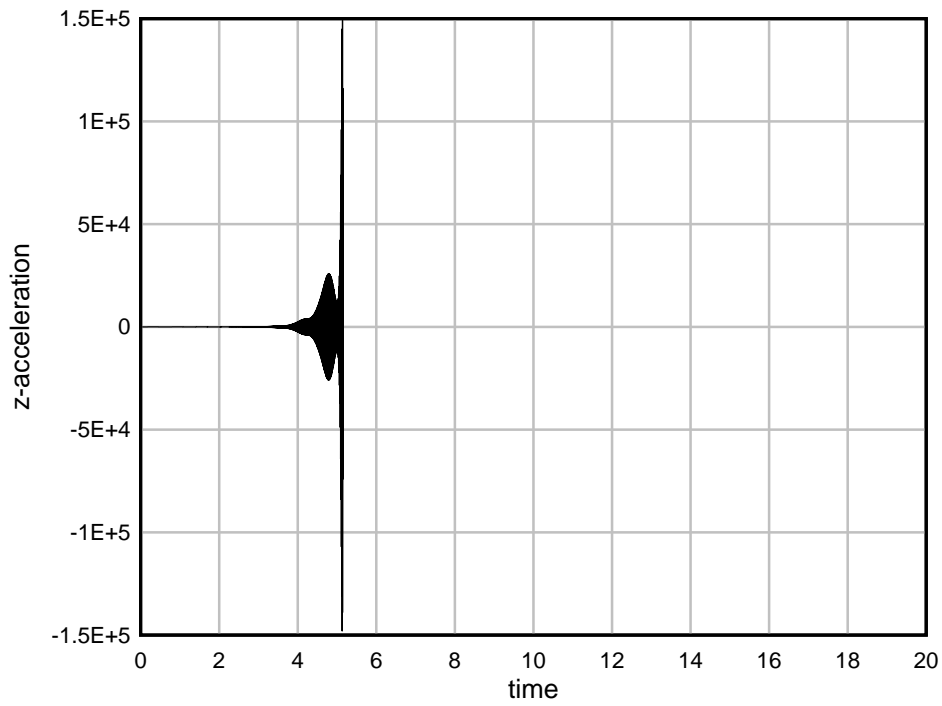


Figure 4.14. Acceleration of the numerical compound pendulum model using the trapezoidal rule,

$$E = 2 \times 10^{11} \text{ N/m}^2, \Delta t = 0.005 \text{ s}$$

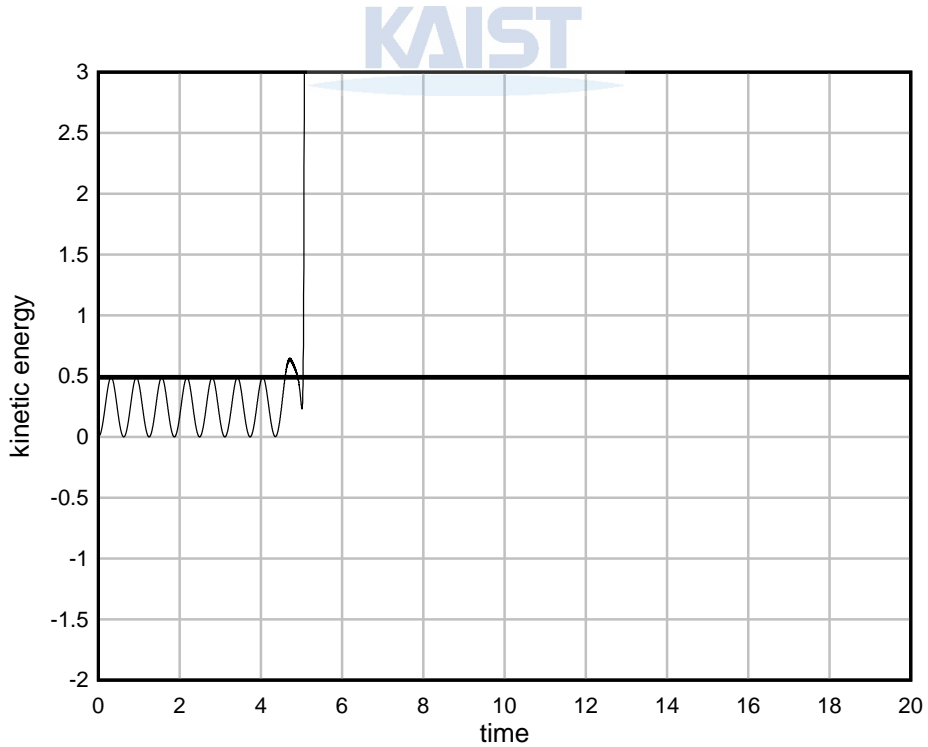


Figure 4.15. Kinetic energy of the numerical compound pendulum model using the trapezoidal rule,

$$E = 2 \times 10^{11} \text{ N/m}^2, \Delta t = 0.005 \text{ s} . \text{ Straight reference line indicates initial potential energy.}$$

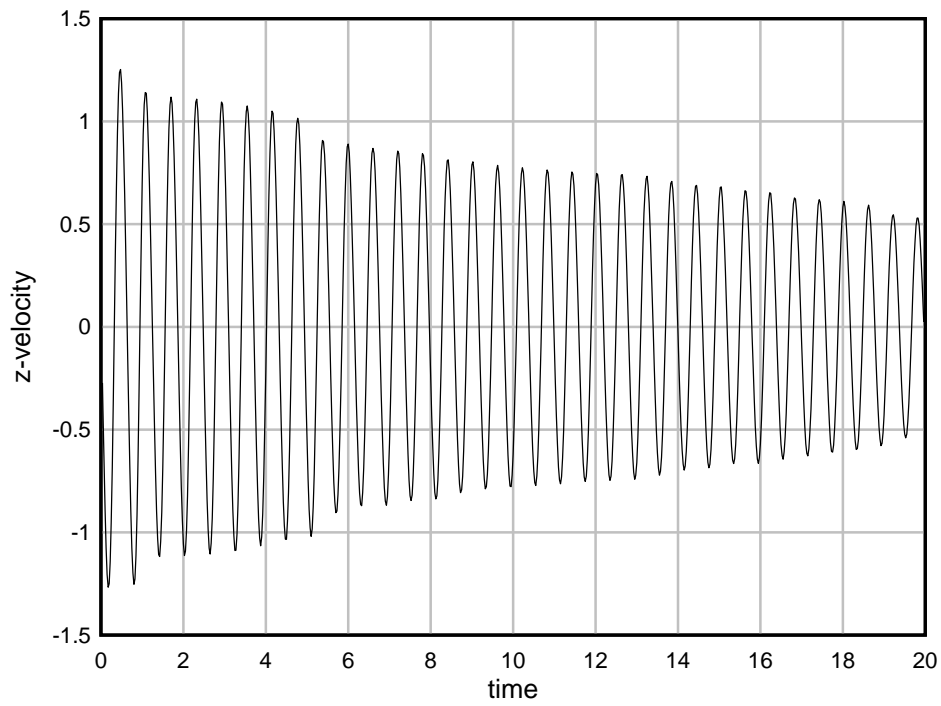


Figure 4.16. Velocity of the numerical compound pendulum model using two-substep Newmark(0.6,0.5)

method, $E = 6 \times 10^{11} \text{ N/m}^2$, $\Delta t = 0.05 \text{ s}$

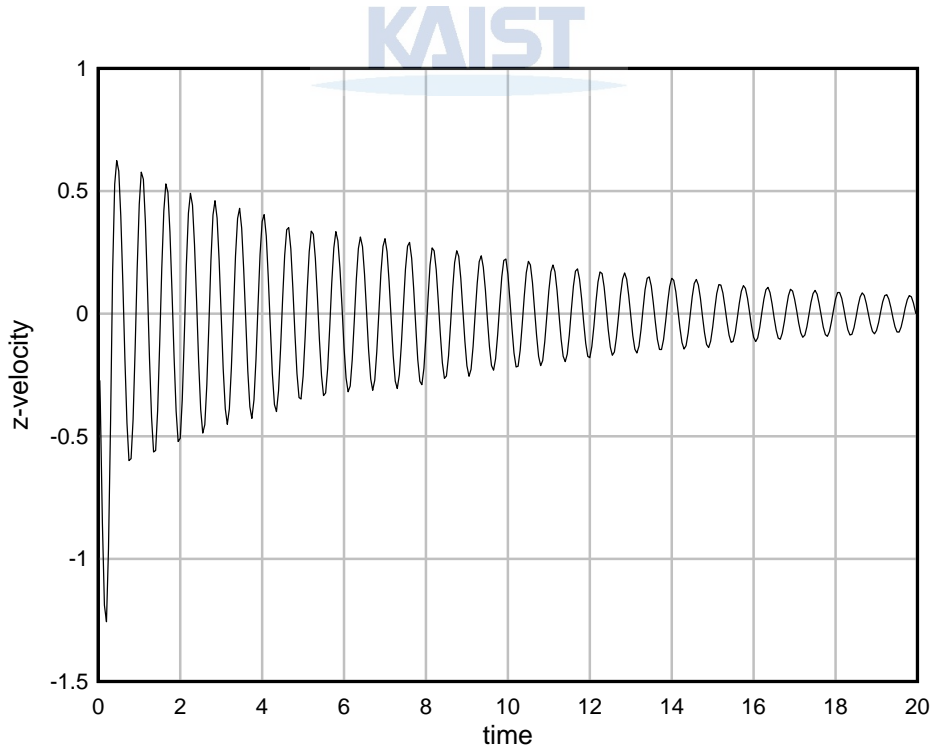


Figure 4.17. Velocity of the numerical compound pendulum model using Bathe composite method,

$E = 6 \times 10^{11} \text{ N/m}^2$, $\Delta t = 0.05 \text{ s}$

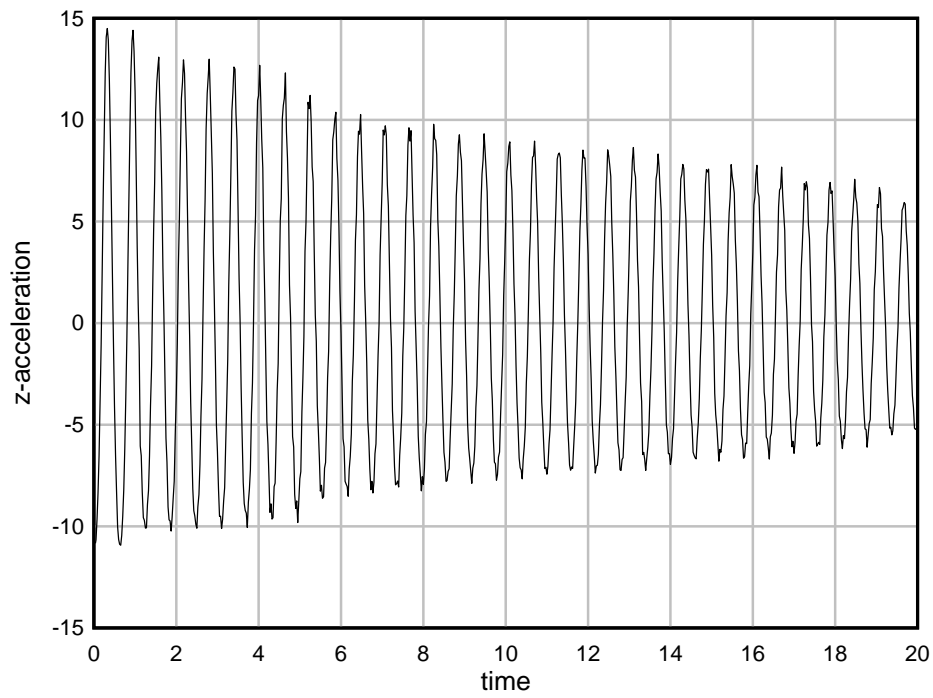


Figure 4.18. Acceleration of the numerical compound pendulum model using two-substep Newmark(0.6,0.5)

method, $E = 6 \times 10^{11} \text{ N/m}^2$, $\Delta t = 0.05 \text{ s}$

KAIST

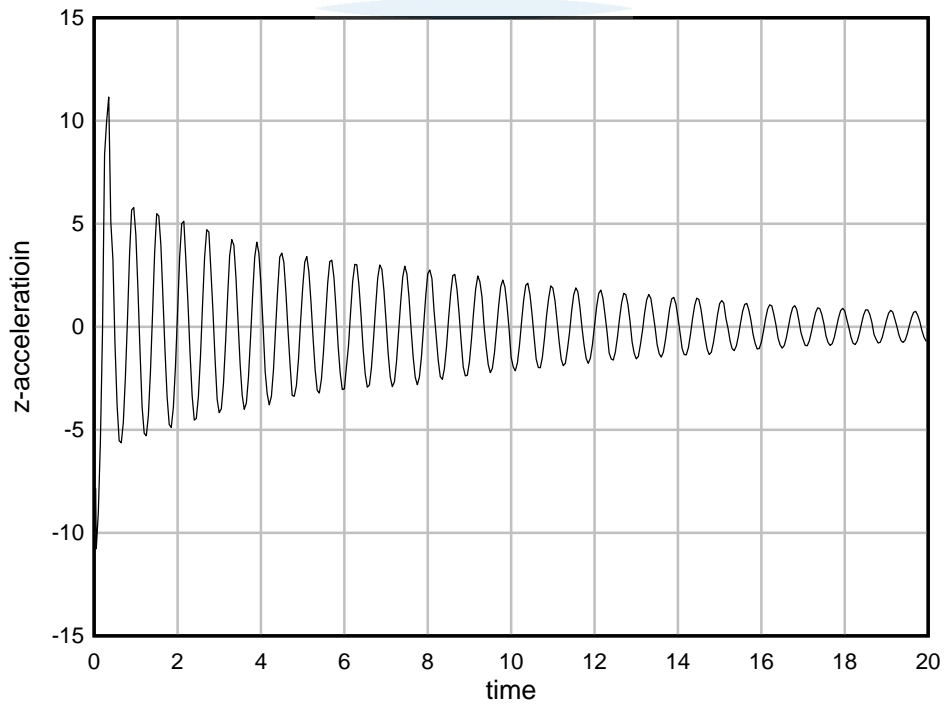


Figure 4.19. Acceleration of the numerical compound pendulum model using Bathe composite method,

$E = 6 \times 10^{11} \text{ N/m}^2$, $\Delta t = 0.05 \text{ s}$

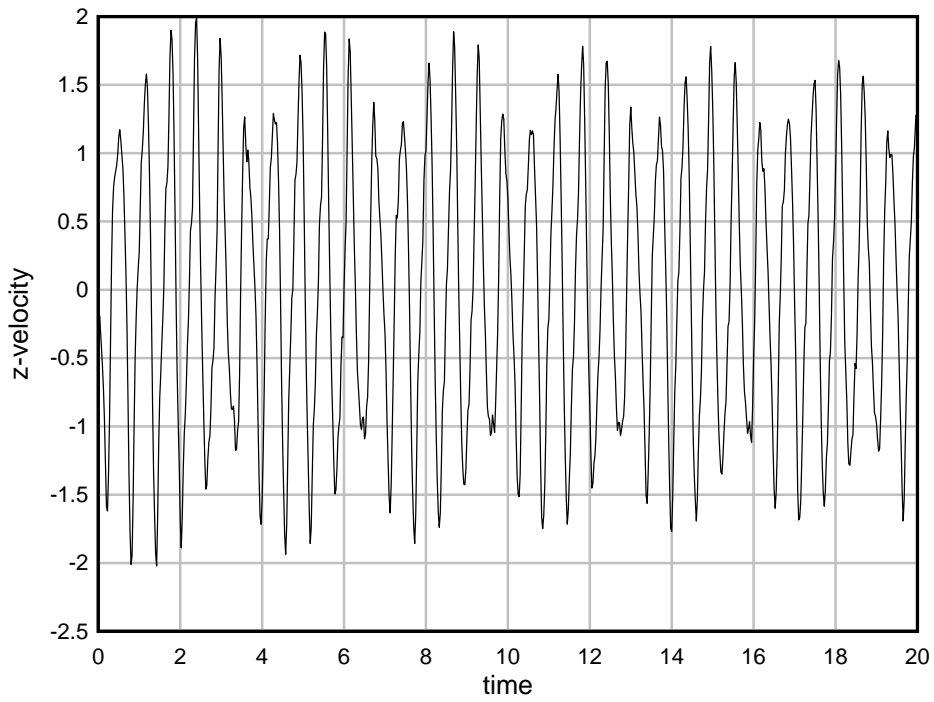


Figure 4.20. Velocity of the numerical compound pendulum model using two-substep Newmark(0.6,0.5)

method, $E = 1 \times 10^7 \text{ N/m}^2$, $\Delta t = 0.05 \text{ s}$

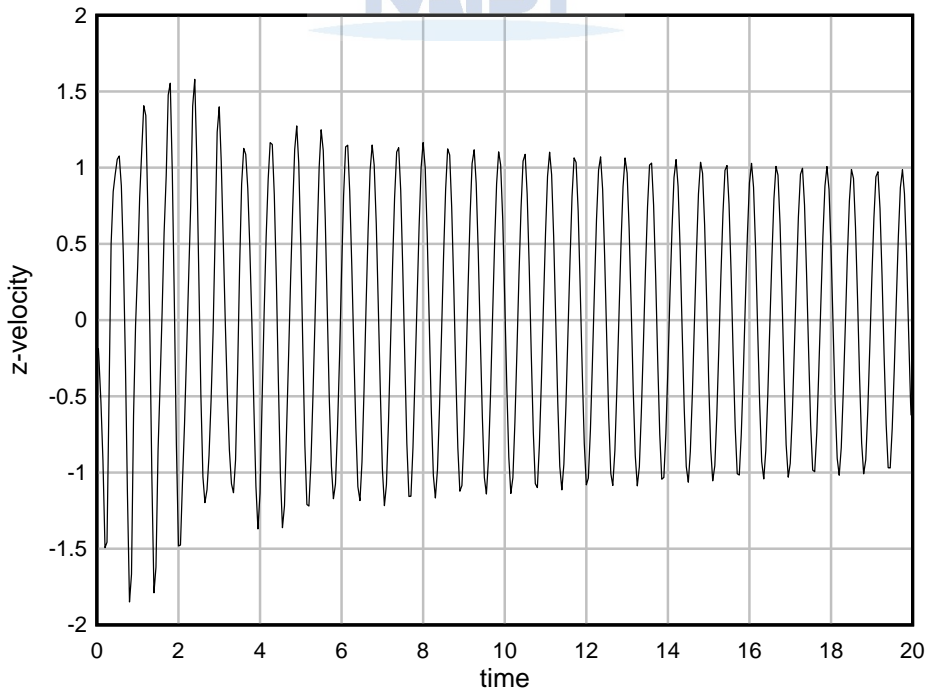


Figure 4.21. Velocity of the numerical compound pendulum model using Bathe composite method,

$E = 1 \times 10^7 \text{ N/m}^2$, $\Delta t = 0.05 \text{ s}$

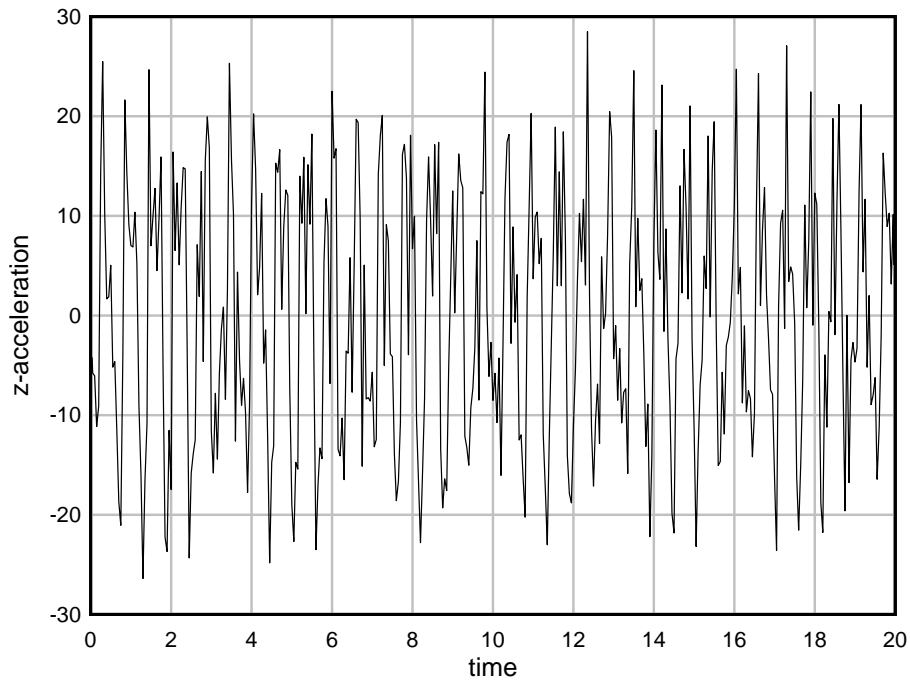


Figure 4.22. Acceleration of the numerical compound pendulum model using two-substep Newmark(0.6,0.5)

method, $E = 1 \times 10^7 \text{ N/m}^2$, $\Delta t = 0.05 \text{ s}$

KAIST

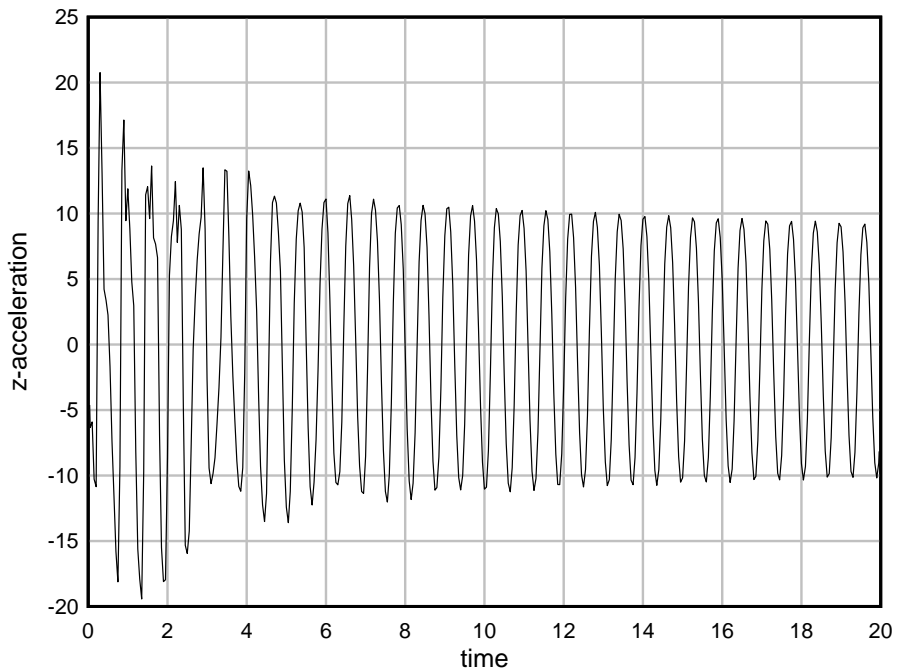


Figure 4.23. Acceleration of the numerical compound pendulum model using Bathe composite method,

$E = 1 \times 10^7 \text{ N/m}^2$, $\Delta t = 0.05 \text{ s}$

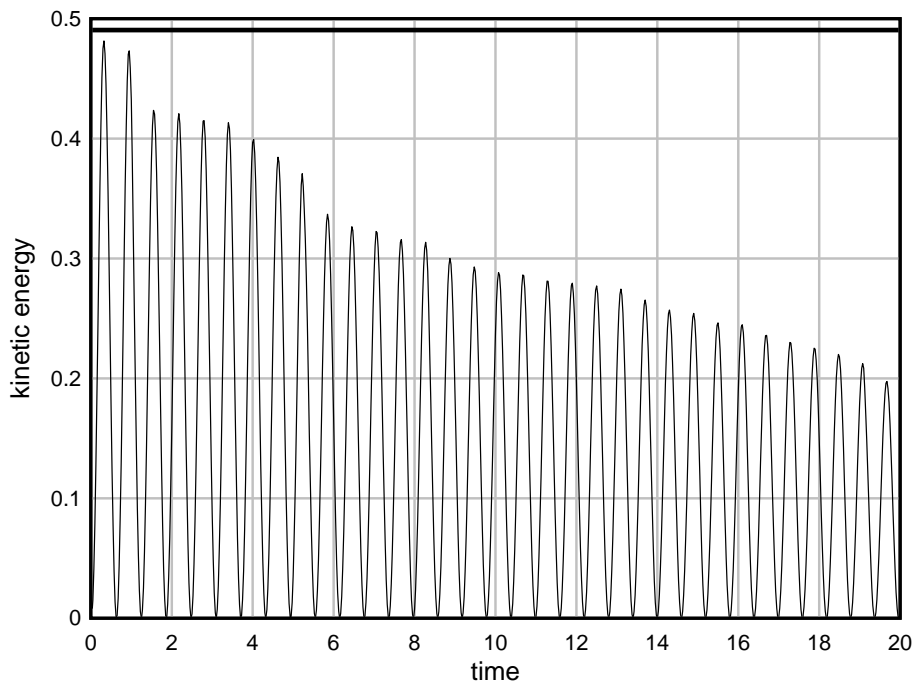


Figure 4.24. Kinetic energy of the numerical compound pendulum model using two-substep Newmark(0.6,0.5) method, $E = 6 \times 10^{11} \text{ N/m}^2$, $\Delta t = 0.05 \text{ s}$. Straight reference line indicates initial potential energy.

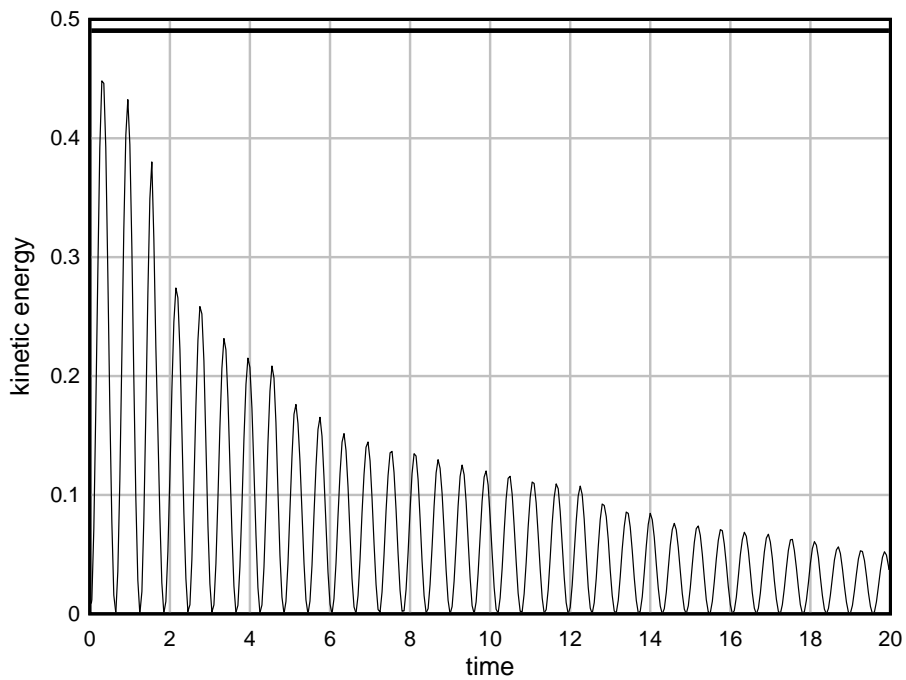


Figure 4.25. Kinetic energy of the numerical compound pendulum model using Bathe composite method, $E = 6 \times 10^{11} \text{ N/m}^2$, $\Delta t = 0.05 \text{ s}$. Straight reference line indicates initial potential energy.

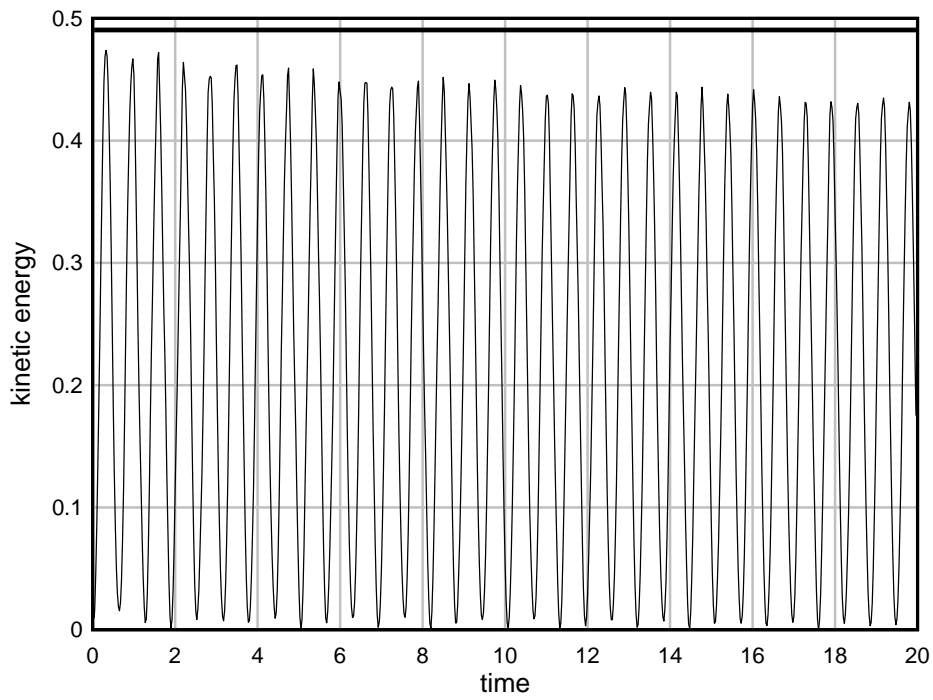


Figure 4.26. Kinetic energy of the numerical compound pendulum model using two-substep Newmark(0.6,0.5) method, $E = 1 \times 10^7 \text{ N/m}^2$, $\Delta t = 0.05 \text{ s}$. Straight reference line indicates initial potential energy.

KAIST

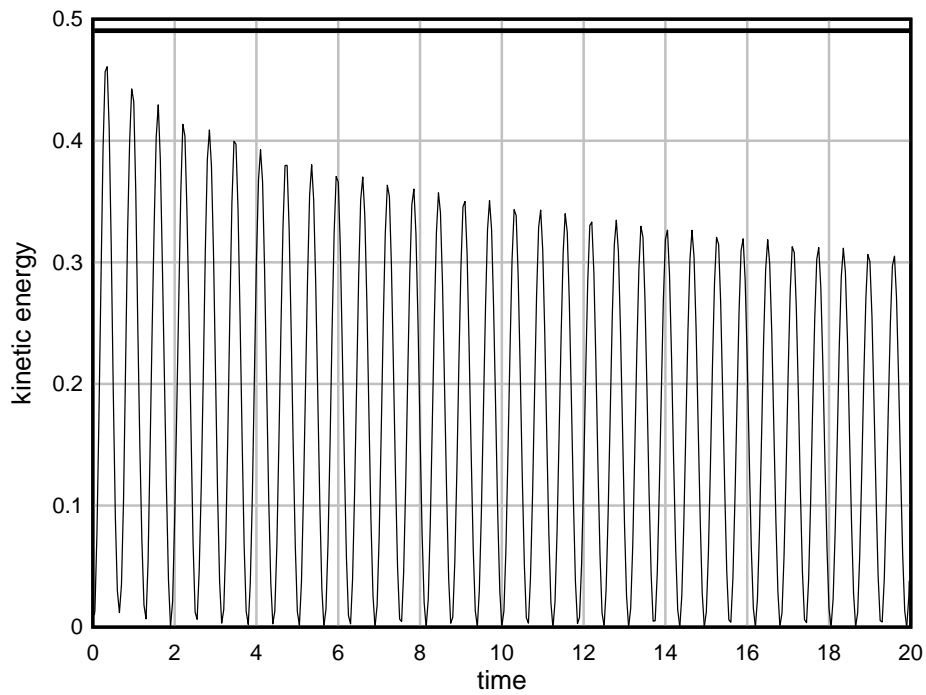


Figure 4.27. Kinetic energy of the numerical compound pendulum model using Bathe composite method, $E = 1 \times 10^7 \text{ N/m}^2$, $\Delta t = 0.05 \text{ s}$. Straight reference line indicates initial potential energy.

4.3 Cantilever beam

We solve cantilever beam in [7]. It is modeled with 400 nine-node two-dimensional solid elements, one element in the thickness direction and 400 elements in the longitudinal direction. It is subjected to (displacement-dependent) pressure load on the top side.

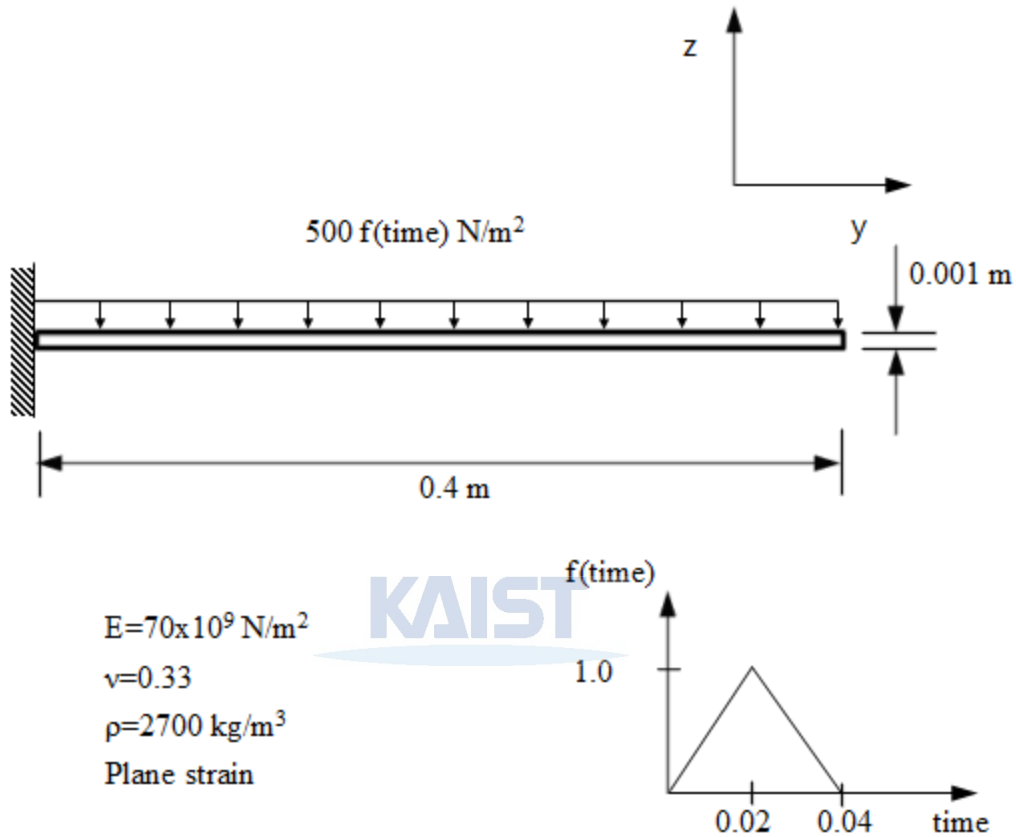


Figure 4.28. Schema and description of the numerical cantilever beam model

Table 4.3. Choice of parameter of numerical cantilever beam for the evaluation of performance

Method	Parameter	Step size (Δt)
The trapezoidal rule	-	0.002s
Two-substep Newmark	(0.5001,0.5) and (0.6,0.5)	0.004s
Bathe composite	-	0.004s

The trapezoidal rule was used to show instability of the numerical cantilever beam model. For two-substep Newmark and Bathe composite method, twice the step size for the trapezoidal rule was used. Because both of the two methods are two-substep method, we used essentially the same step size for all the methods in

real computation.

Fig. 4.29 to 4.40 shows displacement, velocity and acceleration of the methods in Table 4.3.

Displacement, velocity and acceleration response of numerical cantilever beam shows that Bathe composite method exhibit slightly more decay than two-substep Newmark method. It means that period elongation is better than numerical damping for analysis of numerical cantilever beam problem.

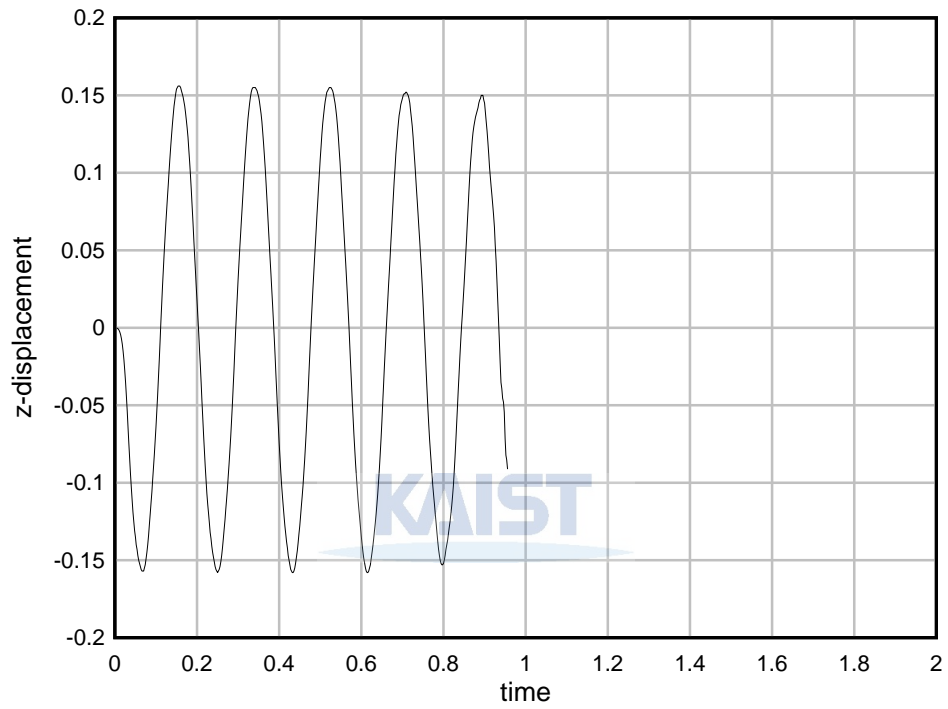


Figure 4.29. Displacement of the numerical cantilever beam model using the trapezoidal rule, $\Delta t = 0.002s$

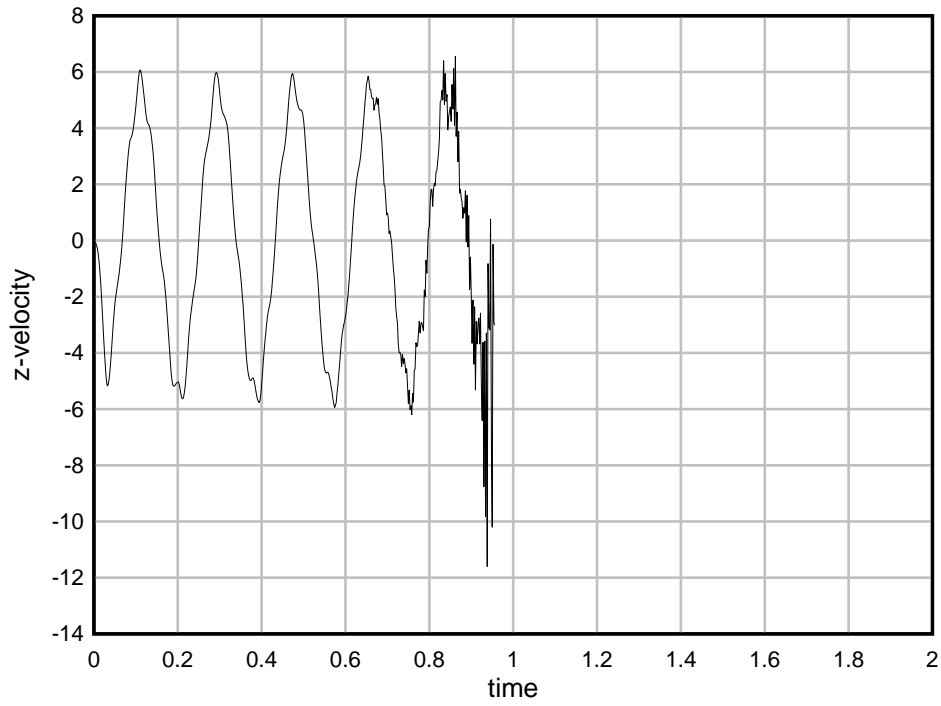


Figure 4.30. Velocity of the numerical cantilever beam model using the trapezoidal rule, $\Delta t = 0.002s$

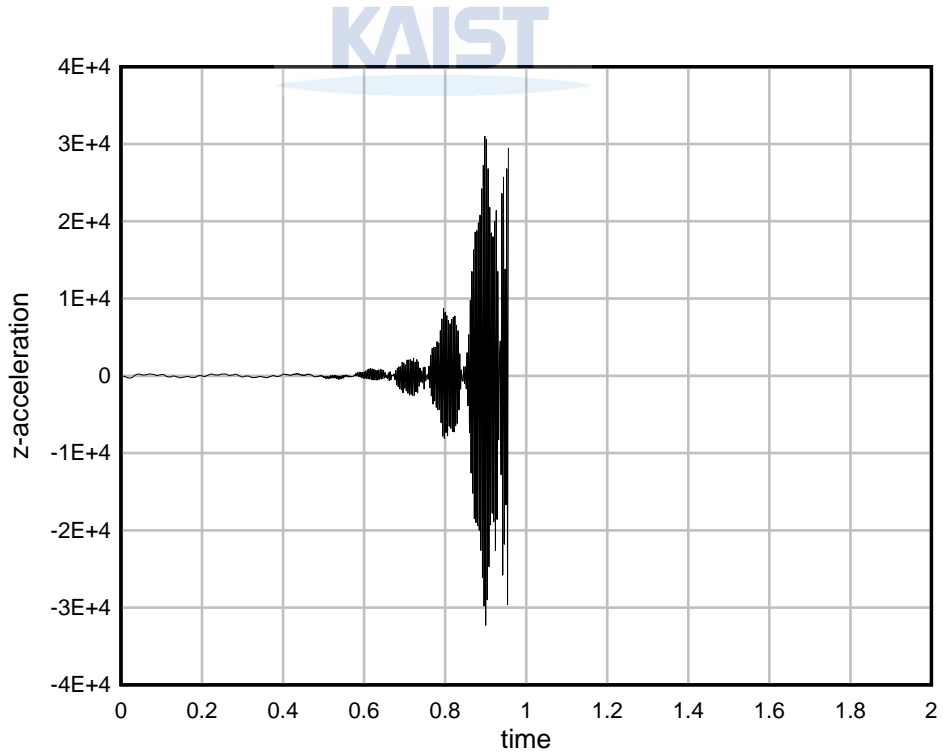


Figure 4.31. Acceleration of the numerical cantilever beam model using the trapezoidal rule, $\Delta t = 0.002s$

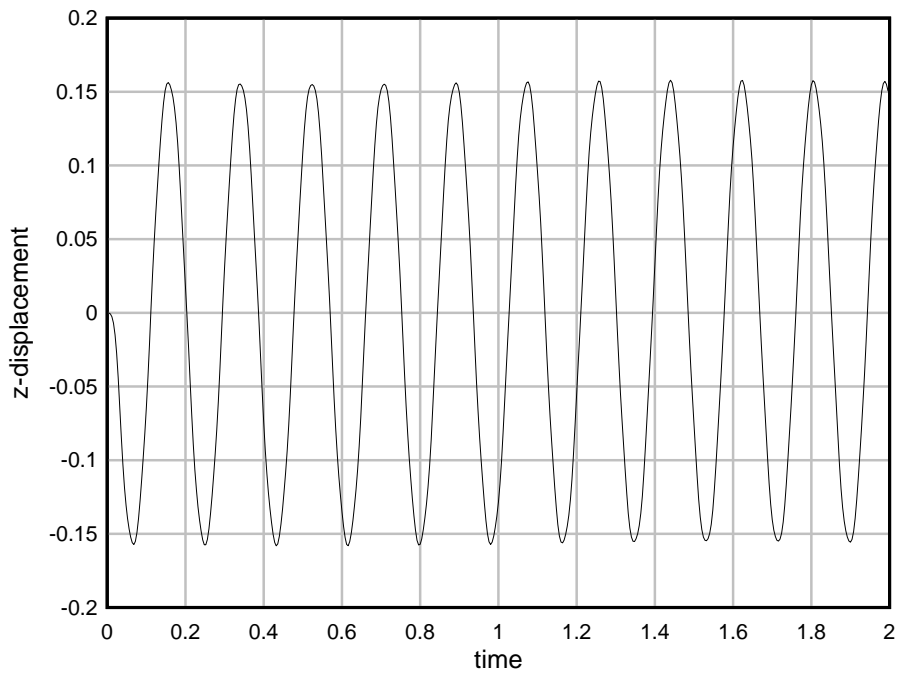


Figure 4.32. Displacement of the numerical cantilever beam model using two-substep Newmark(0.5001,0.5) method, $\Delta t = 0.004s$

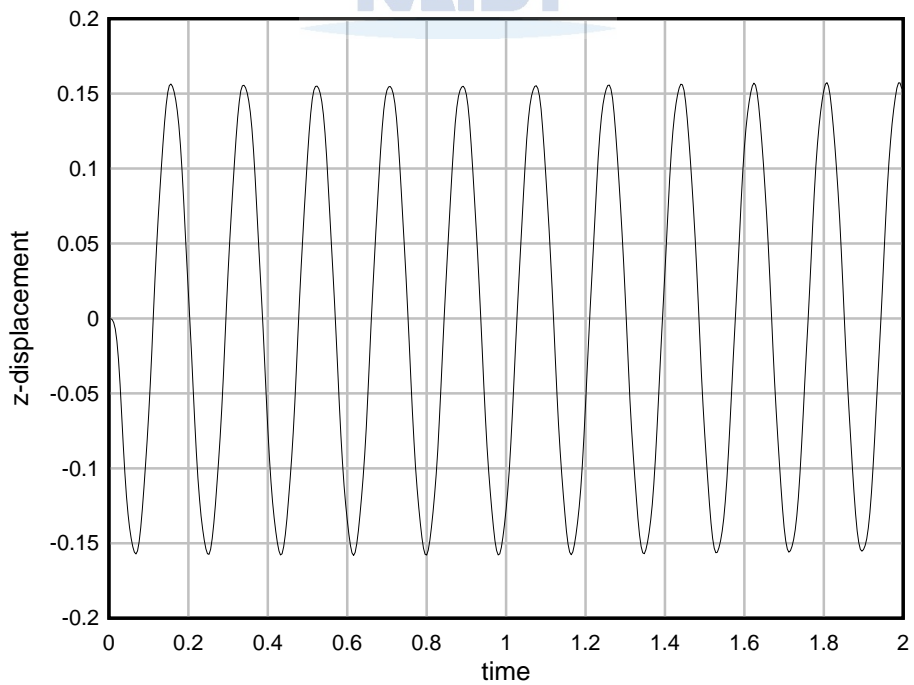


Figure 4.33. Displacement of the numerical cantilever beam model using two-substep Newmark(0.6,0.5) method, $\Delta t = 0.004s$

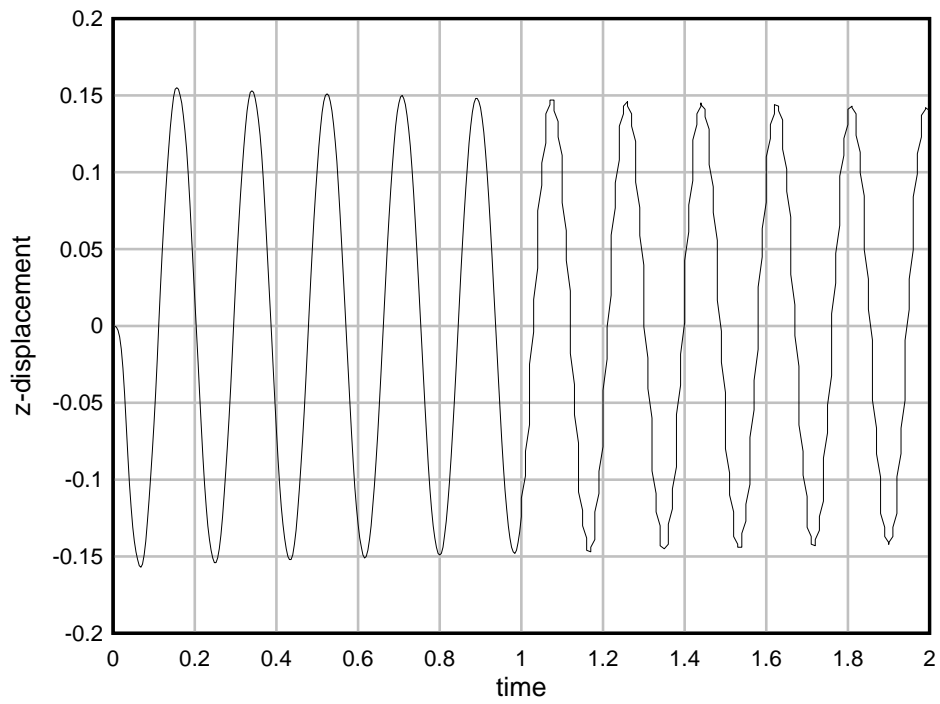


Figure 4.34. Displacement of the numerical cantilever beam model using Bathe composite method,

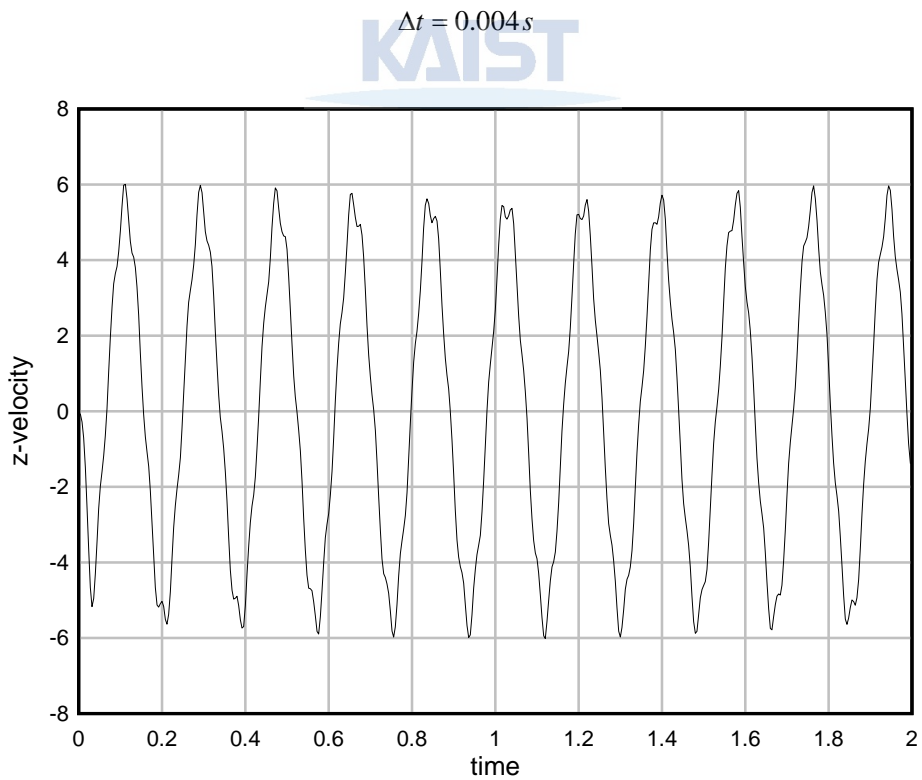


Figure 4.35. Velocity of the numerical cantilever beam model using two-substep Newmark(0.5001,0.5) method, $\Delta t = 0.004s$

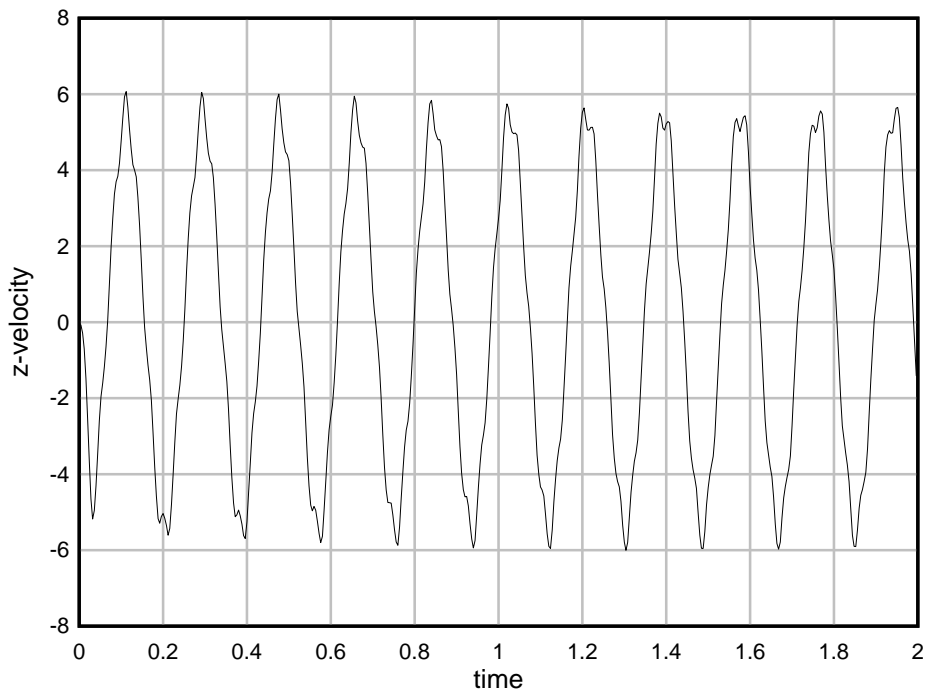


Figure 4.36. Velocity of the numerical cantilever beam model using two-substep Newmark(0.6,0.5) method,

$$\Delta t = 0.004 s$$

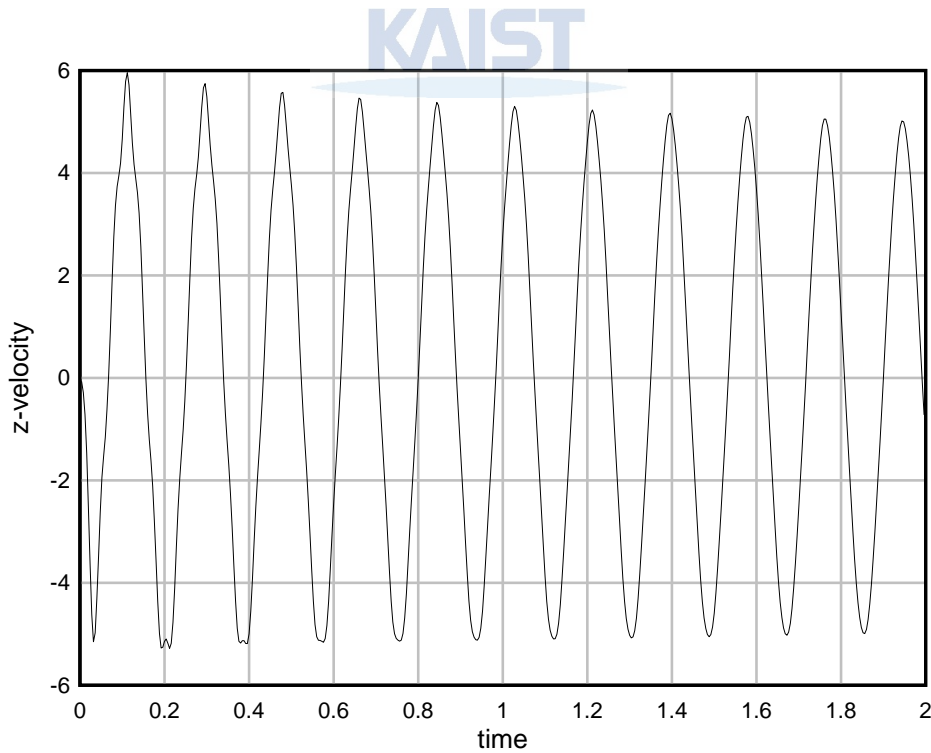


Figure 4.37. Velocity of the numerical cantilever beam model using Bathe composite method, $\Delta t = 0.004 s$

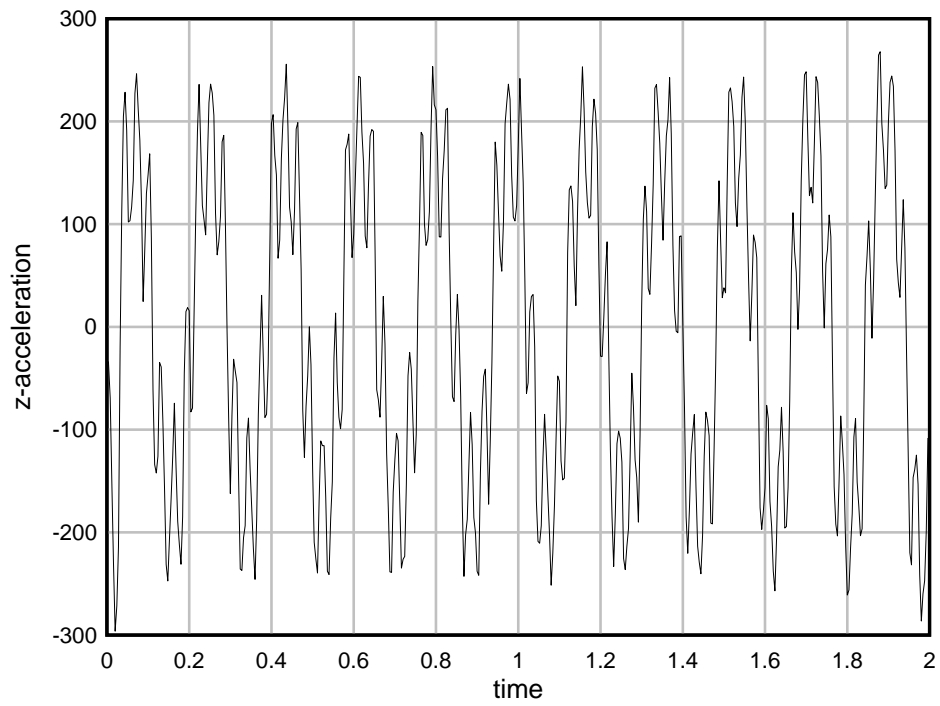


Figure 4.38. Acceleration of the numerical cantilever beam model using two-substep Newmark(0.5001,0.5) method, $\Delta t = 0.004s$

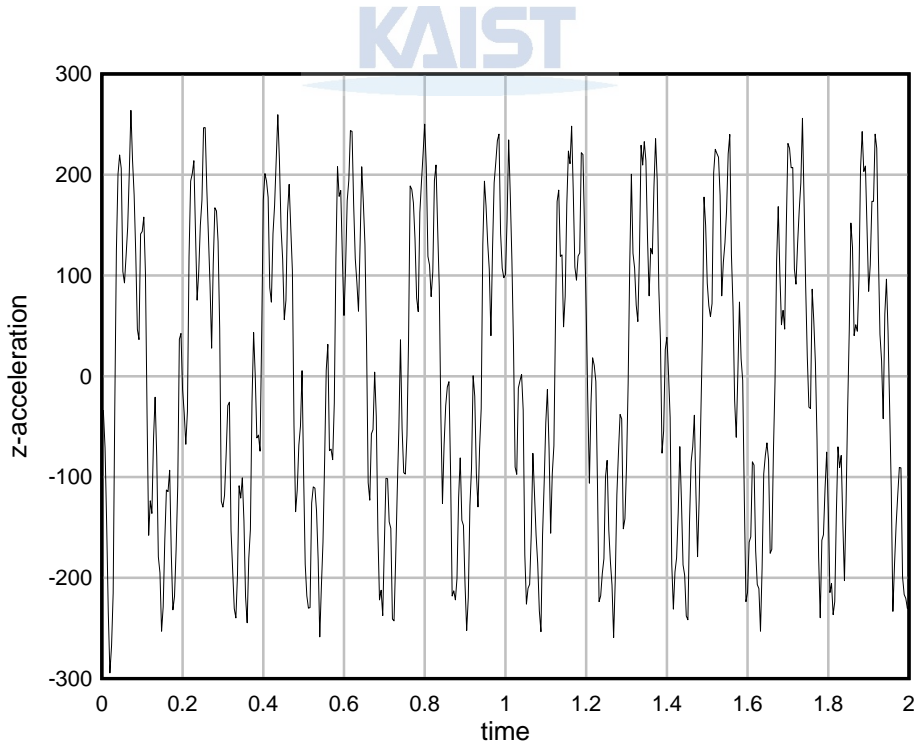


Figure 4.39. Acceleration of the numerical cantilever beam model using two-substep Newmark(0.6,0.5) method, $\Delta t = 0.004s$

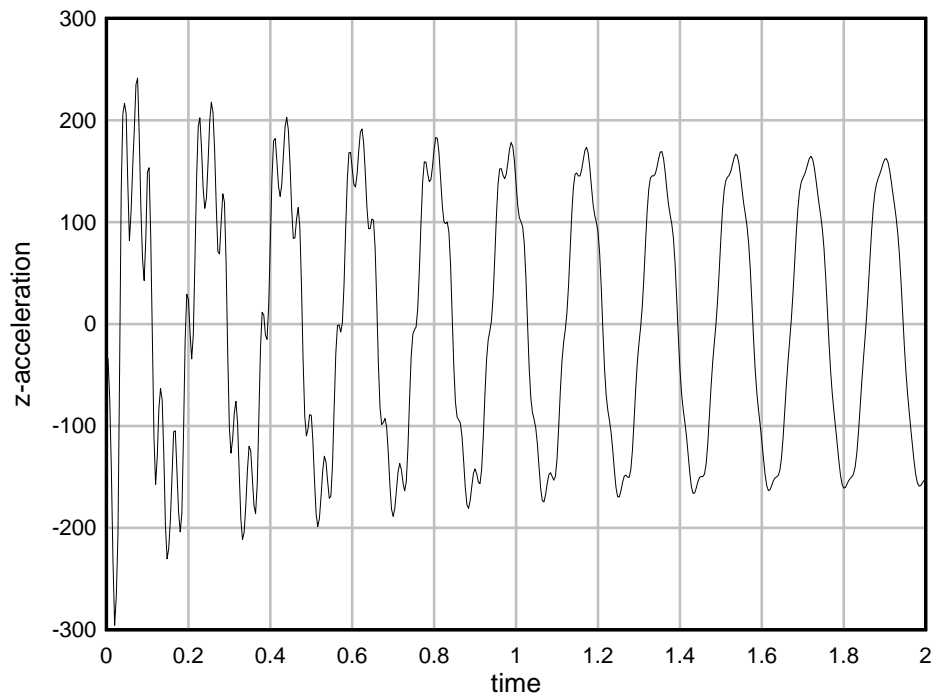


Figure 4.40. Acceleration of the numerical cantilever beam model using Bathe composite method,

$$\Delta t = 0.004 s$$

KAIST

4.4 Cylindrical shell

Kuhl([4],[13]) observed convergence problem of EMM to create methods with numerical damping, CEMM and GEMM. This example was designed to follow closely the cylindrical shell in [4] and [13]. Eight-node isoparametric shell element with five degrees of freedom per node with 2x2 Gauss integration per element was used. Because rotation degrees of freedom are used just to correctly update director vectors per element, physical boundary condition was applied to translational degrees of freedom only. Because the director vectors are set default by ADINA, and because of difference in shell formulation from [4] and [13], response is slightly different with the references.

two methods are two-substep method, we used essentially the same step size for all the methods in real computation.

Fig. 4.42 to 4.46 shows displacement of the methods in Table 4.4.

Displacement response of numerical cylindrical shell shows two things, i.e. buckling and post-buckling vibration. Two displacements at the center line of hinged boundaries of cylindrical shell shows that the initially convex model becomes concave, and vibrates in that concave circumstance. As the entire structure fluctuate, amplitude of vibration at the center line decreases until stabilized vibration of constant amplitude occurs. When the trapezoidal rule is used, solution is stopped shortly after displacement undergoes stabilized vibration.

Among the candidate methods, Bathe composite method shows the most good stabilized vibration in terms of large amplitude and its preservation. For two-substep Newmark method, parameter (0.6,0.5) was better than (0.55,0.5) while both of them use period elongation and no numerical damping. It turned out that method with numerical damping is more suitable for solving the numerical cylindrical shell model than that of period elongation. For two-substep Newmark method, parameter (0.55,0.55) was better than both parameter (0.55,0.5) and (0.6,0.5) that the post-buckling vibration has high and preserved amplitude at the stabilized range of time. Notice that post-buckling vibration of two-substep Newmark (0.55,0.55) and Bathe composite are almost the same. By adjusting the parameters in two-substep Newmark, we could almost catch up the performance of Bathe composite.

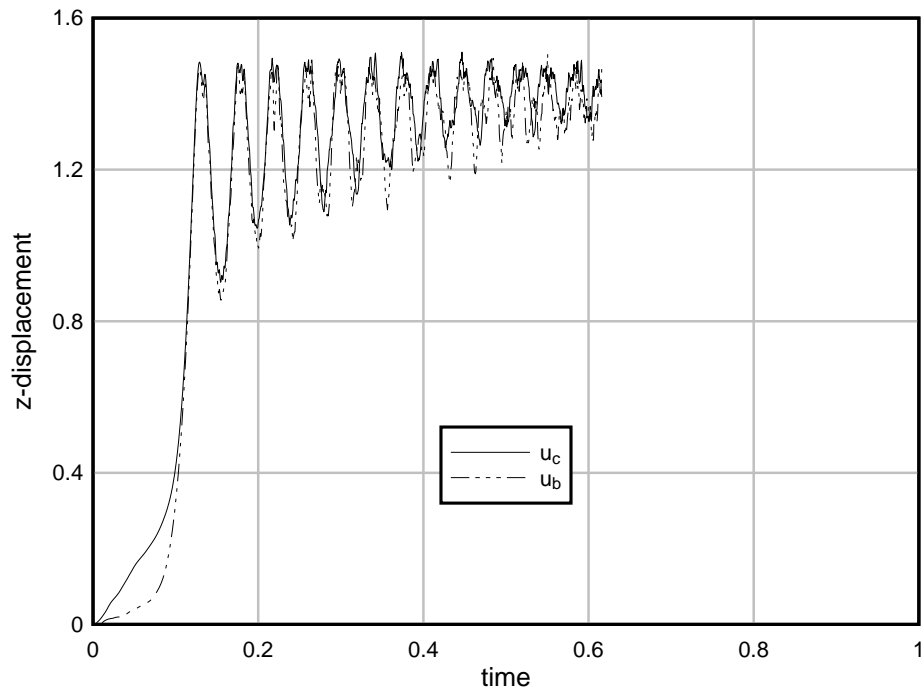


Figure 4.42. Displacement of the numerical cylindrical shell model using the trapezoidal rule, $\Delta t = 0.0005s$

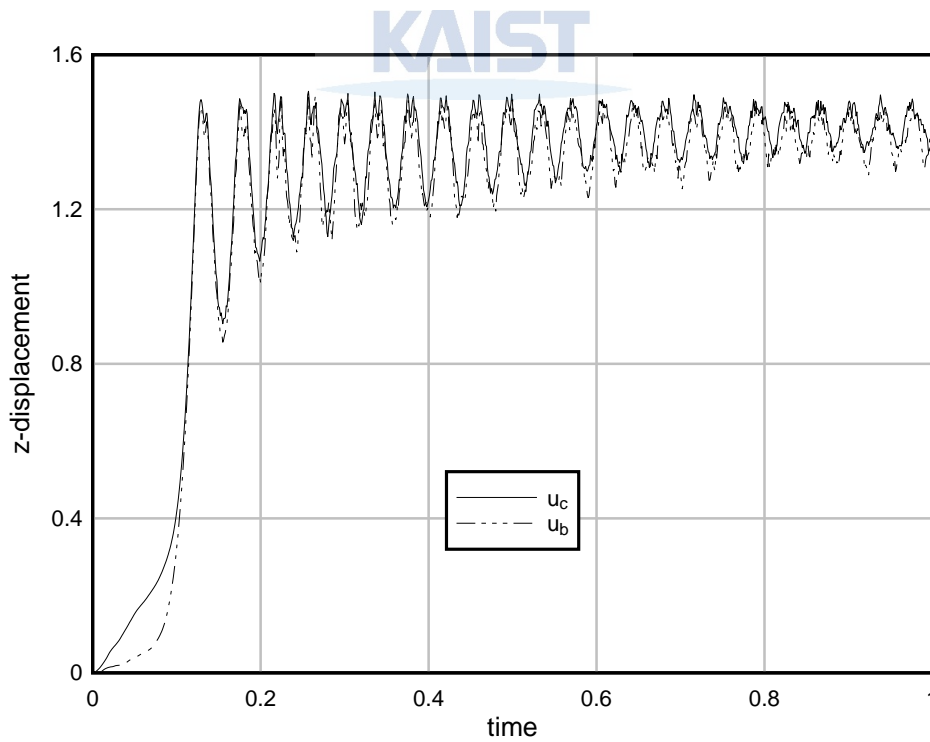


Figure 4.43. Displacement of the numerical cylindrical shell model using two-substep Newmark(0.6,0.5) method, $\Delta t = 0.001s$

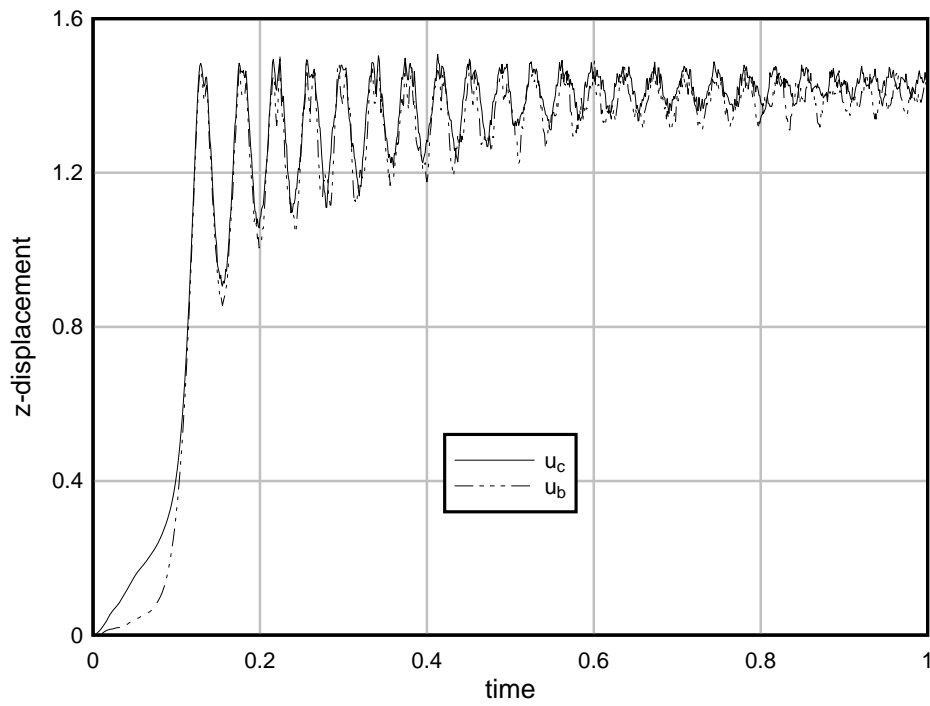


Figure 4.44. Displacement of the numerical cylindrical shell model using two-substep Newmark(0.55,0.5) method, $\Delta t = 0.001s$

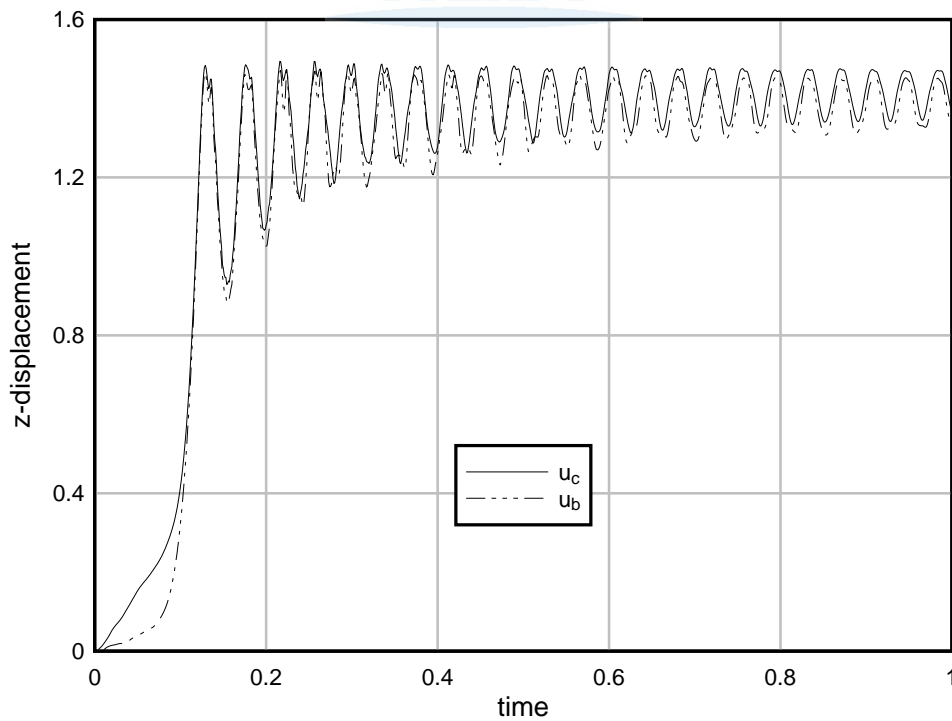


Figure 4.45. Displacement of the numerical cylindrical shell model using two-substep Newmark(0.55,0.5) method, $\Delta t = 0.001s$

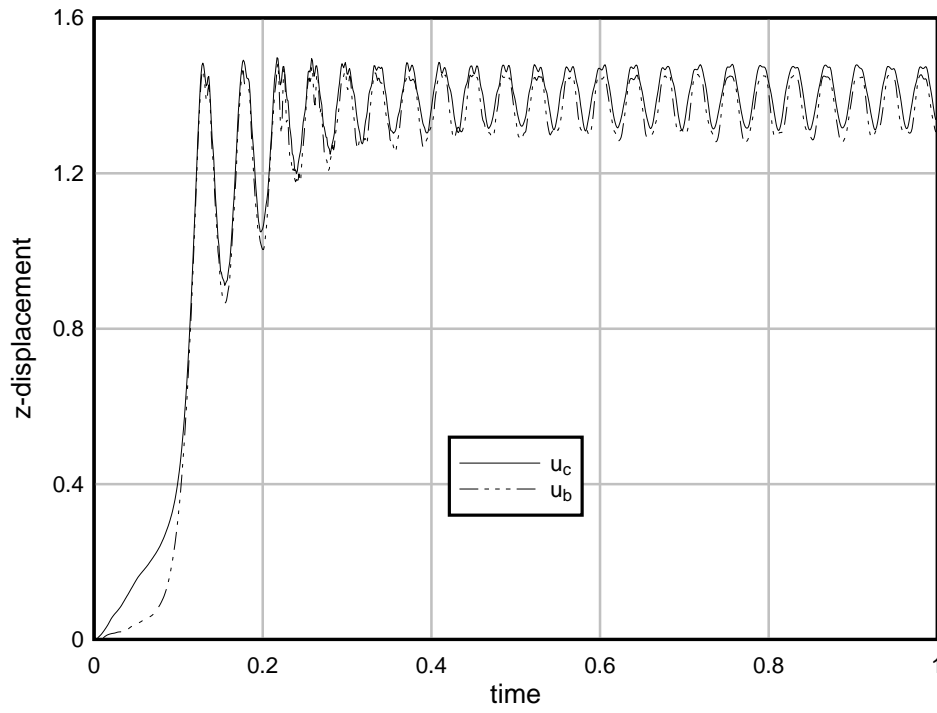


Figure 4.46. Displacement of the numerical cylindrical shell model using Bathe composite method,

$\Delta t = 0.001s$

Chapter 5. Conclusion

We have studied various parameter values of Newmark time integration method into non-linear dynamic problems with instability. We have observed that parameter of Newmark time integration is meaningful for solving such instabilities. Increase of β_0 in Newmark(β_0, β_1) method from the trapezoidal rule gives method with period elongation, and increase of β_1 in Newmark(β_0, β_1) method from the trapezoidal rule gives method with numerical damping. Strength at accuracy of choosing period elongation or numerical damping depends on each problem of nonlinear instability. Therefore, a wise choice between numerical damping and period elongation is required for any time integration method. Most of all, very few method have only period elongation without numerical damping like Newmark($\beta_0, 0.5$). Further study of Newmark($\beta_0, 0.5$) will aid in development of new time integration method in the future.



Appendix

KAIST

Chapter A. Formulation of shell elements

We present here non-linear four-node shell element with five degrees of freedom per node. To Clarify, Configuration at time $t + \Delta t$ and time t in here means the last and the previous of each iteration. Therefore, processes in this section should be used to update (2.44), (2.45) and (2.47) per each iteration.

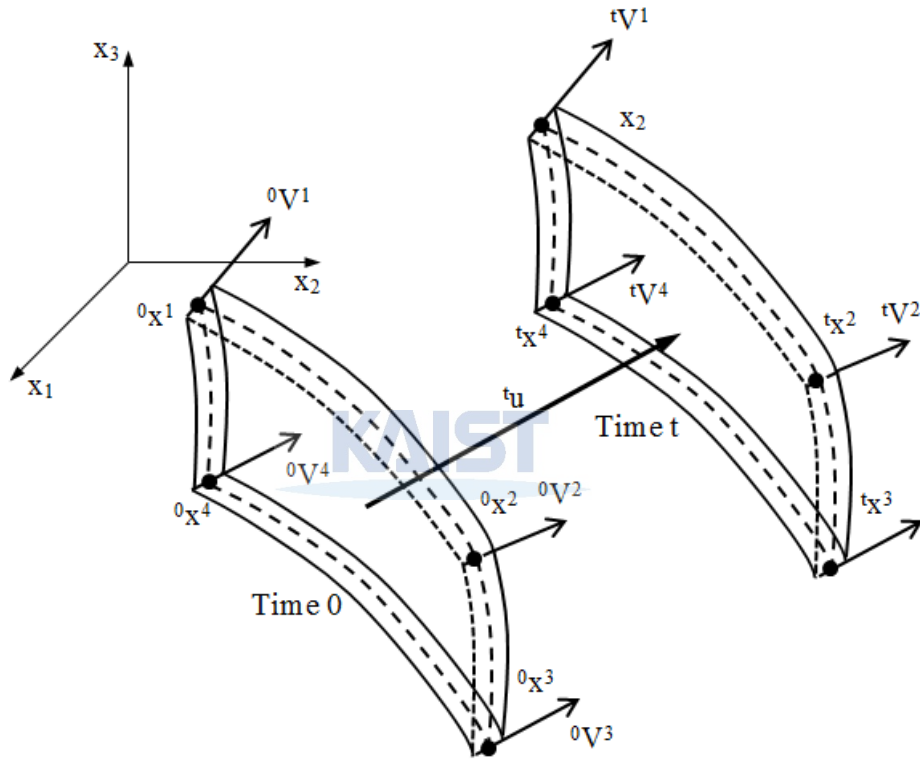


Figure A.1. Initial and current geometry of shell element

Geometry of initial and current configuration is interpolated like below.

$${}^0x_i = \sum_{k=1}^4 h_k {}^0x_i^k + \frac{r_3}{2} a \sum_{k=1}^4 h_k {}^0V_i^k \quad (\text{A.1})$$

$${}^tx_i = \sum_{k=1}^4 h_k {}^tx_i^k + \frac{r_3}{2} a \sum_{k=1}^4 h_k {}^tV_i^k \quad (\text{A.2})$$

Here right superscript on x denotes node number, so too the right subscript on h . h is shape function common for isoparametric elements, with natural coordinates r_1 and r_2 . r_3 is the third natural coordi-

nate, and a is thickness of the shell. The natural coordinates range from -1 to 1 and cover entire geometry for each configuration.

Besides the Cartesian coordinate system, two more coordinate system should be given for each configuration: covariant coordinate system and local Cartesian coordinate system.

For configuration l , covariant bases are defined as

$${}^l\vec{g}_i = \frac{\partial {}^l\vec{x}}{\partial r_i} \quad (\text{A.3})$$

The set of three vectors $\{{}^l\vec{g}_1, {}^l\vec{g}_2, {}^l\vec{g}_3\}$ form a basis. Notice that this basis changes not only by configuration, but also within the element geometry. This covariant basis is for computing strains within the element. Also notice from the definition covariant base vectors follow the line of increasing the respective natural coordinates.

Another basis is local Cartesian basis, which can be calculated from covariant basis like below. We first normalize the three vectors in covariant basis.

$${}^l\vec{e}_{r,i} = \frac{{}^l\vec{g}_i}{\|{}^l\vec{g}_i\|} \quad (\text{A.4})$$

The vectors in the set $\{{}^l\vec{e}_{r,1}, {}^l\vec{e}_{r,2}, {}^l\vec{e}_{r,3}\}$ are now of unit length, but they are not orthogonal to each other. We make a set of orthogonal vectors,

$${}^l\vec{e}_3 = {}^l\vec{e}_{r,3}, {}^l\vec{e}_1 = ({}^l\vec{e}_{r,2} \times {}^l\vec{e}_{r,3}) / \|{}^l\vec{e}_{r,2} \times {}^l\vec{e}_{r,3}\|, {}^l\vec{e}_2 = ({}^l\vec{e}_{r,3} \times {}^l\vec{e}_1) / \|{}^l\vec{e}_{r,3} \times {}^l\vec{e}_1\| \quad (\text{A.5})$$

The set of resulting vectors $\{{}^l\vec{e}_1, {}^l\vec{e}_2, {}^l\vec{e}_3\}$ are now orthonormal to each other. This basis is called local Cartesian basis. Notice from (A.1) and (A.2) the third natural coordinate is always perpendicular to the mid-surface of the shell. Local Cartesian basis is composed of three orthonormal vectors with third vector always in the direction of increasing the third natural coordinate. Therefore, this basis can be used for applying material law for the element.

On the other hand, any basis has its dual basis. Dual basis of covariant basis $\{{}^l\vec{g}_i\}$ is called contravariant basis $\{{}^l\vec{G}_i\}$, which is defined like below.

$${}^l\vec{g}_i \bullet {}^l\vec{G}_j = \delta_{ij} \quad (\text{A.6})$$

For Cartesian and local Cartesian basis, dual basis is itself. This concept of dual basis is used for transforming strains. For example, consider that strain components are given for covariant component and contravariant basis and we want to transform it into local Cartesian basis $\{{}^l\vec{e}_i\}$, i.e. we want to know the compo-

nents of the same strain in local Cartesian coordinate. Because strain is a second-order tensor, writing covariant component as ${}^l\bar{\varepsilon}_{ij}$ and local Cartesian components as ${}^l\varepsilon_{ij}$, following equation is satisfied.

$$\underline{\underline{{}^l\varepsilon}} = {}^l\bar{\varepsilon}_{ij} {}^l\vec{G}_i \otimes {}^l\vec{G}_j = {}^l\varepsilon_{rs} {}^l\vec{e}_r \otimes {}^l\vec{e}_s \quad (\text{A.7})$$

From this, unknown components in local Cartesian basis is,

$${}^l\varepsilon_{ij} = {}^l\vec{e}_i \bullet ({}^l\varepsilon_{rs} {}^l\vec{e}_r \otimes {}^l\vec{e}_s) \bullet {}^l\vec{e}_j = {}^l\vec{e}_i \bullet ({}^l\bar{\varepsilon}_{rs} {}^l\vec{G}_r \otimes {}^l\vec{G}_s) \bullet {}^l\vec{e}_j = {}^l\bar{\varepsilon}_{ij} ({}^l\vec{e}_i \bullet {}^l\vec{G}_r) ({}^l\vec{e}_j \bullet {}^l\vec{G}_s) \quad (\text{A.8})$$

If known and unknown are reversed, we similarly apply dot product for the dual basis of known component to the basis of unknown component.

$${}^l\bar{\varepsilon}_{ij} = {}^l\vec{g}_i \bullet ({}^l\varepsilon_{rs} {}^l\vec{e}_r \otimes {}^l\vec{e}_s) \bullet {}^l\vec{g}_j = {}^l\vec{g}_i \bullet ({}^l\varepsilon_{rs} {}^l\vec{e}_r \otimes {}^l\vec{e}_s) \bullet {}^l\vec{g}_j = {}^l\varepsilon_{rs} ({}^l\vec{g}_i \bullet {}^l\vec{e}_r) ({}^l\vec{g}_j \bullet {}^l\vec{e}_s) \quad (\text{A.9})$$

Now let us assume every configuration from time 0 to time t is known. We want to solve for incremental displacement \vec{u} to get to the unknown configuration at time $t + \Delta t$, as in the following equation.

$${}^{t+\Delta t}\vec{u} = {}^t\vec{u} + \vec{u} \quad (\text{A.10})$$

Notice that not only the coordinates at the nodes, but also the change in director vectors \vec{V}^k should be given for each configuration. This is done by adopting two rotational degrees of freedom α_k and β_k per each node. Using small-rotations, director vectors in unknown configuration is given by

$${}^{t+\Delta t}\vec{V}^k = {}^t\vec{V}^k + \vec{V}^k \quad (\text{A.11})$$

$$\vec{V}^k = -{}^t\vec{V}_2^k \alpha_k + {}^t\vec{V}_1^k \beta_k \quad (\text{A.12})$$

Where ${}^t\vec{V}_1^k$ and ${}^t\vec{V}_2^k$ are vectors orthogonal to ${}^t\vec{V}^k$ defined as

$${}^t\vec{V}_1^k \equiv \vec{e}_2 \times {}^t\vec{V}^k / \|\vec{e}_2 \times {}^t\vec{V}^k\| \quad (\text{A.13})$$

$${}^t\vec{V}_2^k \equiv {}^t\vec{V}^k \times \vec{V}_1^k \quad (\text{A.14})$$

where \vec{e}_2 is the second Cartesian basis. The rotation degrees of freedom are not accumulated and just used to update the vector ${}^{t+\Delta t}\vec{V}^k$. At the start of each iteration where configuration at time $t + \Delta t$ is solved from previous information, values of α_k and β_k are reset to zero. Also, vectors ${}^t\vec{V}_1^k$ and ${}^t\vec{V}_2^k$ are recalculated at the start of each iteration using (A.13) and (A.14).

Because (2.43) was formulated in Cartesian system, it is also applied to local Cartesian system. Therefore, let us assume (2.43) is written in local Cartesian system. Material law for used in (2.43) is defined for local Cartesian stress $\underline{\underline{\sigma}}_{ij}$ and strain $\underline{\underline{\varepsilon}}_{ij}$ components,

$$\underline{\underline{C}} = \frac{E}{1-\nu^2} \begin{pmatrix} 1 & \nu & 0 & 0 & 0 & 0 \\ & 1 & 0 & 0 & 0 & 0 \\ & & 0 & 0 & 0 & 0 \\ & & & \frac{1-\nu}{2} & 0 & 0 \\ & & & & k(\frac{1-\nu}{2}) & 0 \\ \text{Sym.} & & & & & k(\frac{1-\nu}{2}) \end{pmatrix} \quad (\text{A.15})$$

$$\vec{\sigma} = \underline{\underline{C}} \vec{\varepsilon} \quad (\text{A.16})$$

$$\vec{\sigma}^T = (\sigma_{11} \quad \sigma_{22} \quad \sigma_{33} \quad \sigma_{12} \quad \sigma_{23} \quad \sigma_{31}) \quad (\text{A.17})$$

$$\vec{\varepsilon}^T = (\varepsilon_{11} \quad \varepsilon_{22} \quad \varepsilon_{33} \quad 2\varepsilon_{12} \quad 2\varepsilon_{23} \quad 2\varepsilon_{31}) \quad (\text{A.18})$$

To calculate the matrices in (2.43) in local Cartesian system, we need to know both total and incremental strains. We use total strain in calculating stresses ${}^t_0 \underline{\underline{S}}_{ij}$ identifying ${}^t_0 \underline{\underline{S}}_{ij} = \sigma_{ij}$ in (A.16). Second, we use incremental strains to calculate $\underline{\underline{B}}_L$ and $\underline{\underline{N}}_{NL}$. To do so, we start from covariant strain component.

Covariant strain component at the previous of current configuration is given by,

$${}^t_0 \underline{\underline{\varepsilon}}_{ij} = \frac{1}{2} ({}^t \vec{g}_i \bullet {}^t \vec{g}_j - {}^0 \vec{g}_i \bullet {}^0 \vec{g}_j) \quad (\text{A.19})$$

Using (A.19) with (A.8) and (A.16), we calculate ${}^t_0 \underline{\underline{S}}_{ij}$, which is used to approximate ${}^{t+\Delta t}_0 \underline{\underline{S}}_{ij}$ in the iterative equilibrium of (2.43).

We need incremental strain in linear and nonlinear part respectively, which are reproduced in following equations.

$${}^{t+\Delta t}_0 \underline{\underline{\varepsilon}}_{ij} = {}^t_0 \underline{\underline{\varepsilon}}_{ij} + {}_0 \underline{\underline{\varepsilon}}_{ij} \quad (\text{A.20})$$

$${}_0 \underline{\underline{\varepsilon}}_{ij} = {}_0 \underline{\underline{e}}_{ij} + {}_0 \underline{\underline{\eta}}_{ij} \quad (\text{A.21})$$

On the other hand, using (A.19) with (A.3) gives alternative form of (A.19).

$${}^t_0 \underline{\underline{\varepsilon}}_{ij} = \frac{1}{2} ({}^t \vec{u}_{,i} \bullet {}^0 \vec{g}_j + {}^0 \vec{g}_i \bullet {}^t \vec{u}_{,j} + {}^t \vec{u}_{,i} \bullet {}^t \vec{u}_{,j}) \quad (\text{A.22})$$

where the convention ${}^t \vec{u}_{,i} = \frac{\partial {}^t \vec{u}}{\partial r_i}$ is used. Using (A.22) into (A.20),

$${}_0 \underline{\underline{\varepsilon}}_{ij} = \frac{1}{2} (\vec{u}_{,i} \bullet {}^0 \vec{g}_j + {}^0 \vec{g}_i \bullet \vec{u}_{,j} + \vec{u}_{,i} \bullet {}^t \vec{u}_{,j} + {}^t \vec{u}_{,i} \bullet \vec{u}_{,j} + \vec{u}_{,i} \bullet \vec{u}_{,j}) \quad (\text{A.23})$$

Using again the definition of (A.3),

$${}_0 \underline{\underline{\varepsilon}}_{ij} = \frac{1}{2} (\vec{u}_{,i} \bullet {}^t \vec{g}_j + {}^t \vec{g}_i \bullet \vec{u}_{,j} + \vec{u}_{,i} \bullet \vec{u}_{,j}) \quad (\text{A.24})$$

It can be separated into linear and nonlinear part in (A.21),

$${}^0\bar{e}_{ij} = \frac{1}{2}(\bar{\vec{u}}_i \bullet {}^t\bar{\vec{g}}_j + {}^t\bar{\vec{g}}_i \bullet \bar{\vec{u}}_j) \quad (\text{A.25})$$

$${}^0\bar{\eta}_{ij} = \frac{1}{2}(\bar{\vec{u}}_i \bullet \bar{\vec{u}}_j) \quad (\text{A.26})$$

Comparing (2.31) and (A.25), notice that the form of linear incremental strain is simpler because we expressed it in covariant components. Recall that we need matrices related to linear incremental strain and virtual non-linear incremental strain,

$${}^0e_{ij_e} = \underline{\underline{B}}_L \Delta U_e \quad (\text{A.27})$$

$$\delta_0 \eta_{ij_e} = \delta U_e^T \underline{\underline{N}}_{NL} \Delta U_e \quad (\text{A.28})$$

In fact, we do not need closed form of $\underline{\underline{B}}_L$ and $\underline{\underline{N}}_{NL}$. Instead, using (A.8), we can transform (A.27) and (A.28) into the following equations.

$${}^0\bar{e}_{ij_e} = \overline{\underline{\underline{B}}_L} \Delta U_e \quad (\text{A.27})$$

$$\delta_0 \bar{\eta}_{ij_e} = \delta U_e^T \overline{\underline{\underline{N}}_{NL}} \Delta U_e \quad (\text{A.28})$$

Now we deal with the form of $\overline{\underline{\underline{B}}_L}$ and $\overline{\underline{\underline{N}}_{NL}}$.

For the four-node element considered, elemental nodal incremental displacement vector ΔU_e can be expressed in a following form.

$$\Delta U_e^T = \begin{pmatrix} u_1^1 & u_1^2 & u_1^3 & u_1^4 & u_2^1 & u_2^2 & u_2^3 & u_2^4 & u_3^1 & u_3^2 & u_3^3 & u_3^4 \\ \alpha_1 & \alpha_2 & \alpha_3 & \alpha_4 & \beta_1 & \beta_2 & \beta_3 & \beta_4 \end{pmatrix} \quad (\text{A.29})$$

Using (A.2), (A.10) and (A.12) form of incremental displacement is

$$u_i = \sum_{k=1}^4 h_k u_i^k + \frac{r_3}{2} a \sum_{k=1}^4 h_k (-{}^tV_{2i}^k \alpha_k + {}^tV_{i1}^k \beta_k) \quad (\text{A.31})$$

Derivatives of incremental displacement in terms of natural coordinates can be expressed as,

$$\frac{\partial \bar{\vec{u}}}{\partial r_i} = \underline{\underline{D}}_i \Delta U_e \quad (\text{A.32})$$

$\underline{\underline{D}}_i$ is 3x20 matrix which is easily calculated from (A.31). Using (A.25),

$${}^0\bar{e}_{ij_e} = \frac{1}{2}({}^t\bar{\vec{g}}_j^T \underline{\underline{D}}_i + {}^t\bar{\vec{g}}_i^T \underline{\underline{D}}_j) \Delta U_e \quad (\text{A.33})$$

Using (A.28),

$$\delta_0 \bar{\eta}_{ij_e} = \delta U_e^T \frac{1}{2} (\underline{\underline{D}}_i^T \underline{\underline{D}}_j + \underline{\underline{D}}_j^T \underline{\underline{D}}_i) \Delta U_e \quad (\text{A.34})$$

From (A.33) and (A.34), we get closed form of $\underline{\underline{B}}_L$ and $\underline{\underline{N}}_{NL}$.

To prevent shear locking, we should use the covariant strains in modified form, called ‘assumed covariant strains’. In covariant components, only the transverse shear strains are modified. The incremental strains in (A.27) and (A.28), and the total strain in (A.19) should be modified as in the following equations.

$${}^0\bar{e}_{23e}^{AS} = \frac{1}{2}(1+r_1){}^0\bar{e}_{23e}(1,0,r_3) + \frac{1}{2}(1-r_1){}^0\bar{e}_{23e}(-1,0,r_3) \quad (\text{A.35})$$

$${}^0\bar{e}_{31e}^{AS} = \frac{1}{2}(1+r_2){}^0\bar{e}_{31e}(0,1,r_3) + \frac{1}{2}(1-r_2){}^0\bar{e}_{31e}(0,-1,r_3) \quad (\text{A.36})$$

$$\delta_0 \bar{\eta}_{23e}^{AS} = \frac{1}{2}(1+r_1)\delta_0 \bar{\eta}_{23e}(1,0,r_3) + \frac{1}{2}(1-r_1)\delta_0 \bar{\eta}_{23e}(-1,0,r_3) \quad (\text{A.37})$$

$$\delta_0 \bar{\eta}_{31e}^{AS} = \frac{1}{2}(1+r_2)\delta_0 \bar{\eta}_{31e}(0,1,r_3) + \frac{1}{2}(1-r_2)\delta_0 \bar{\eta}_{31e}(0,-1,r_3) \quad (\text{A.38})$$

$${}^t\bar{\mathcal{E}}_{23}^{AS} = \frac{1}{2}(1+r_1){}^t\bar{\mathcal{E}}_{23}(1,0,r_3) + \frac{1}{2}(1-r_1){}^t\bar{\mathcal{E}}_{23}(-1,0,r_3) \quad (\text{A.39})$$

$${}^t\bar{\mathcal{E}}_{31}^{AS} = \frac{1}{2}(1+r_2){}^t\bar{\mathcal{E}}_{31}(0,1,r_3) + \frac{1}{2}(1-r_2){}^t\bar{\mathcal{E}}_{31}(0,-1,r_3) \quad (\text{A.40})$$

Parentheses after each strains means substitution of the natural coordinates.

KAIST

References

- [1] Park, K.C. (1975), "An improved stiffly stable method for direct integration of nonlinear structural dynamic equations", *ASME J. Appl. Mech.*, 42, pp. 404-470.
- [2] Hughes, T.J.R. (1976), "Stability, convergence and growth and decay of energy of the average acceleration method in nonlinear structural dynamics", *Comput. Struct.*, 6, pp. 313-324.
- [3] Baig, M.M.I. et al. (2005), "On direct time integration in large deformation dynamic analysis", *Computational Fluid and Solid mechanics 2005* (K.J. Bathe, ed.), Elsevier, 2005.
- [4] Kuhl, D. et al. (1999), "Generalized Energy-Momentum Method for non-linear adaptive shell dynamics", *Comput. Methods Appl. Mech. Engrg.*, 178, pp. 343-366.
- [5] Hilber, H.M. et al. (1977), "Improved numerical dissipation for time integration algorithms in structural dynamics", *Earthquake Engrg. Struct. Dynam.*, 5, pp. 283-292.
- [6] Liu, T. et al. (2012), "An efficient backward Euler time-integration method for nonlinear dynamic analysis of structures", *Comput. Struct.*, 106-107, pp. 20-28.
- [7] Bathe, K.J. et al. (2005), "On a composite time integration procedure for nonlinear dynamics", *Comput. Struct.*, 83, pp. 2513-2524.
- [8] Bathe, K.J. (2007), "Conserving energy and momentum in nonlinear dynamics: A simple implicit time integration scheme", *Comput. Struct.*, 85, pp. 437-445.
- [9] Crisfield, M.A. et al. (1994), "A co-rotational element/time-integration strategy for non-linear dynamics", *Int. J. Numer. Meth. Engrg.*, 37, pp. 1897-1913.
- [10] Dong, S. (2010), "BDF-like methods for nonlinear dynamic analysis", *Journal of Comput. Physics*, 229, pp. 3019-3045.

- [11] Simo, J.C. et al. (1994), "A new energy and momentum conserving algorithm for the non-linear dynamics of shells", *Int. J. Numer. Meth. Engrg.*, 37, pp. 2527-2549.
- [12] Kuhl, D. et al. (1999), "Energy-conserving and decaying algorithms in non-linear structural dynamics", *Int. J. for Numer. Meth. Engrg.*, 45, pp. 569-599.
- [13] Kuhl, D. et al. (1996), "Constrain Energy Momentum Algorithm and its application to non-linear dynamics of shells", *Comput. Meth. Appl. Mech. Engrg.*, 136, pp. 293-315.
- [14] Simo, J.C. et al. (1992), "The discrete energy-momentum method. Conserving algorithms for nonlinear elastodynamics", *Zeitschrift fur angewandte Mathematik und Physik*, 43, pp. 757-792.
- [15] Chung, J. et al. (1993), "A time integration algorithm for structural dynamics with improved numerical dissipation: The generalized- α method", *J. Appl. Mech.*, 60, pp. 371-375.
- [16] Newmark, N.M. (1959), "A method of computation for structural dynamics", *ASME J. Engrg. Mech.*, 85(EM3), pp. 67-94.
- [17] Bathe, K.J. et al. (2012), "Insight into an implicit time integration scheme for structural dynamics", *Comput. Struct.*, 98-99, pp. 1-6.
- [18] Bathe, K.J. et al. (1973), "Stability and accuracy analysis of direct integration methods", *Earthquake Engrg. Struct. Dynam.*, 1, pp. 283-291.
- [19] Belytschko, T. et al. (1975), "On the unconditional stability of an implicit algorithm for nonlinear structural dynamics", *J. Appl. Mech.*, 42, pp. 865-869.
- [20] Hughes., T.J.R. (1977), "A note on the stability of Newmark's algorithm in non-linear structural dynamics", *Int. J. Numer. Meth. Engrg.*, 11, pp. 383-386.
- [21] Bathe, K.J. (1996). *Finite element procedures*, Prentice Hall, 1037 pages

Summary

Insight into Newmark time integration parameters in non-linear dynamic problems

시간 적분법은 비선형 동적해석을 위한 방법으로 구조물의 거동을 가장 정확하게 표현할 수 있지만 다양한 경우에 대해 불안정성을 갖는다. 그간 불안정성을 없애기 위해 수치 제동을 사용한 시간 적분법이 사용되어 왔지만, 주기 증가를 이용한 방식은 개발되지 않았다. 뉴마크 시간 적분법에 대해 파라미터를 바꾸어 가면 주기 증가를 얻는 알고리즘을 얻을 수 있고 수치 해석을 통해 이것이 불안정성을 안정화하는 데 의미가 있음을 보였다. 이 연구는 향후에 더 나은 시간 적분법을 개발하는 데 사용될 수 있을 것으로 기대된다.

Keywords: Newmark, time integration, Non-linear dynamics, Non-linear instability, Numerical damping, Period elongation

The logo for KAIST (Korea Advanced Institute of Science and Technology) is displayed in a light blue color. It consists of the letters 'KAIST' in a bold, sans-serif font, with a horizontal line underneath the letters.